Available online at www.sciencedirect.com
ScienceDirect
Geochimica et Cosmochimica Acta 73 (2009) 6367–6389
Geochimica et Cosmochimica Acta
www.elsevier.com/locate/gca

Pt–Re–Os and Sm–Nd isotope and HSE and REE systematics of the 2.7 Ga Belingwe and Abitibi komatiites

I.S. Puchtel [a,*], R.J. Walker [a], A.D. Brandon [b], E.G. Nisbet [c]

[a] Department of Geology, University of Maryland, College Park, MD 20742, USA
[b] NASA Johnson Space Center, Houston, TX 77058, USA
[c] Department of Earth Sciences, Royal Holloway, University of London, Egham TW20 0EX, UK

Received 27 March 2009; accepted in revised form 17 July 2009; available online 22 July 2009

Abstract

High-precision Pt–Re–Os and Sm–Nd isotope and highly siderophile element (HSE) and rare earth element (REE) abundance data are reported for two 2.7 b.y. old komatiite lava flows, Tony's flow (TN) from the Belingwe greenstone belt, Zimbabwe, and the PH-II flow (PH) from Munro Township in the Abitibi greenstone belt, Canada. The emplaced lavas are calculated to have contained ~25% (TN) and ~28% (PH) MgO. These lavas were derived from mantle sources characterized by strong depletions in highly incompatible lithophile trace elements, such as light REE ($Ce/Sm_N = 0.64 \pm 0.02$ (TN) and 0.52 ± 0.01 (PH), $\varepsilon^{143}Nd(T) = +2.9 \pm 0.2$ in both sources). ^{190}Pt–^{186}Os and ^{187}Re–^{187}Os isochrons generated for each flow yield ages consistent with respective emplacement ages obtained using other chronometers. The calculated precise initial $^{186}Os/^{188}Os = 0.1198318 \pm 3$ (TN) and 0.1198316 ± 5 (PH) and $^{187}Os/^{188}Os = 0.10875 \pm 17$ (TN) and 0.10873 ± 15 (PH) require time-integrated $^{190}Pt/^{188}Os$ and $^{187}Re/^{188}Os$ of 0.00178 ± 11 and 0.407 ± 8 (TN) and 0.00174 ± 18 and 0.415 ± 5 (PH). These parameters, which by far represent the most precise and accurate estimates of time-integrated Pt/Os and Re/Os of the Archean mantle, are best matched by those of enstatite chondrites. The data also provide evidence for a remarkable similarity in the composition of the sources of these komatiites with respect to both REE and HSE. The calculated absolute HSE abundances in the TN and PH komatiite sources are within or slightly below the range of estimates for the terrestrial Primitive Upper Mantle (PUM). Assuming a chondritic composition of the bulk silicate Earth, the strong depletions in LREE, yet chondritic Re/Os in the komatiite sources are apparently problematic because early Earth processes capable of fractionating the LREE might also be expected to fractionate Re/Os. This apparent discrepancy could be reconciled via a two-stage model, whereby the moderate LREE depletion in the sources of the komatiites initially occurred within the first 100 Ma of Earth's history as a result of either global magma ocean differentiation or extraction and subsequent long-term isolation of early crust, whereas HSE were largely added subsequently via late accretion. The komatiite formation, preceded by derivation of basaltic magmas, was a result of second-stage, large-degree dynamic melting in mantle plumes.

1. INTRODUCTION

Precisely determining the relative and absolute abundances of the highly siderophile elements (HSE; including Re, Os, Ir, Ru, Pt, and Pd) in the mantle is crucial for understanding such fundamental planetary processes as the timing and mechanisms of Earth's primary differentiation of its metallic core from its silicate mantle, as well as possible continued terrestrial accretion following core formation. Absolute HSE abundances, and $^{186}Os/^{188}Os$ and $^{187}Os/^{188}Os$ ratios that reflect the time-integrated Pt/Os and Re/Os in the mantle domains, have previously been estimated for the relatively recent upper mantle via studies of ophiolites,

* Corresponding author. Tel.: +1 301 405 4054; fax: +1 301 405 3597.
E-mail address: ipuchtel@umd.edu (I.S. Puchtel).

0016-7037/$ - see front matter © 2009 Elsevier Ltd. All rights reserved.
doi:10.1016/j.gca.2009.07.022

abyssal peridotites, orogenic lherzolites, and mantle xenoliths (Morgan et al., 1981; Morgan, 1986; Snow and Reisberg, 1995; Rehkämper et al., 1997; Handler and Bennett, 1999; Brandon et al., 2000; Meisel et al., 2001; Pearson et al., 2004; Becker et al., 2006). Most Re–Os isotopic data for mantle materials and mantle-derived lavas suggest that the convecting mantle, on average, has evolved with Re/Os within the range of chondritic meteorites (Shirey and Walker, 1998; Walker, 2009). The more limited Pt–Os isotopic data are likewise consistent with average mantle bearing a long-term Pt/Os within the range of chondritic meteorites (Walker et al., 1997; Brandon et al., 2000, 2006).

Because the HSE have very high (>10,000) and variable low-pressure and temperature metal-silicate partition coefficients (e.g., Jones and Drake, 1986), these elements must have been nearly quantitatively removed from the silicate portion of the Earth following the last major interaction between the core and mantle, leaving the latter with very low and highly fractionated HSE abundances. The generally chondritic relative abundances of the HSE in the mantle, as well as the relatively high absolute abundances of HSE in the mantle, have commonly been attributed to late accretion, a process whereby accretion of ~0.5 wt.% of the Earth continued subsequent to final core segregation (Kimura et al., 1974; Chou et al., 1983; Morgan, 1986). Alternatively, it has also been argued that these characteristics of the HSE might be attributable to metal-silicate partitioning at high temperatures and pressures, such as may occur at the base of a magma ocean (Murthy, 1991; Righter et al., 2000). Discerning which processes most affected the HSE in the mantle will require highly accurate and precise determination of the concentrations of HSE in the bulk mantle, the composition most relevant to issues of planetary differentiation and possible continued accretion (Walker, 2009). Most mantle materials, and the mantle sources of derivative lavas that have been studied for HSE and Os isotopic compositions have, however, been heavily processed via prior melt extraction events and fluid- or melt–rock interactions. Thus, constraining the abundances of the HSE in the bulk mantle has proven problematic (Becker et al., 2006; Lorand et al., 2009).

Komatiites can potentially provide information about HSE in their mantle source(s) and circumvent the mantle modification issues noted above. Most komatiites likely formed via high degrees of partial melting on ascent (Arndt et al., 2008) leading to the extraction of large proportions of the HSE from their mantle sources (Barnes et al., 1985). High degrees of melting provides a mechanism for sampling average mantle that is not possible with small, individual mantle samples, e.g., peridotite xenoliths, or lower degree melts. Because komatiitic magmas are superheated, have low viscosities, and ascend rapidly (Huppert and Sparks, 1985), they undergo little to no differentiation prior to emplacement. Collectively, these characteristics mean that the HSE present in komatiites are potentially much more representative of their mantle sources than the HSE present in melts that are produced by lower degrees of melting and modified by extensive pre-eruption crystal–liquid fractionation, such as most basaltic melts (Rehkämper et al., 1999). The relatively high abundances of HSE in komatiitic liquids also made their HSE much less prone to modification by mantle or crustal contamination. Further, Archean komatiites provide information about the abundances of HSE in the mantle at a time when the mantle was less modified by processes of melt extraction and refertilization via crustal recycling, compared to the modern mantle. Finally, komatiite lava differentiation after emplacement produces a range in Pt/Os, Re/Os, and HSE abundances between different parts of lava flows. This is crucial for obtaining precise chronological information, assess closed-system behaviour of the HSE, and precisely determine absolute and relative HSE abundances in the mantle sources of the lavas.

Several prior studies of Archean komatiites have revealed an apparent discrepancy between their lithophile trace element and HSE systematics. For instance, mantle sources of the 2.7 Ga komatiites from the Pyke Hill area in Canada and 2.9 Ga komatiites from the Volotsk area in Fennoscandia had initial $\varepsilon^{143}Nd = +2.9 \pm 0.2$ and $+2.7 \pm 0.2$, respectively (Puchtel et al., 2004a, 2007), and were derived from sources strongly depleted in light rare earth elements (LREE) and other highly incompatible lithophile trace elements. In contrast, Os isotope data indicate chondritic initial $^{187}Os/^{188}Os$ and $^{186}Os/^{188}Os$, consistent with long-term chondritic Re/Os and Pt/Os in their mantle sources. Puchtel et al. (2007) accounted for this apparent discrepancy via a single-stage model, whereby the komatiite sources initially underwent low-degree partial melting early in Earth history, leading to the removal of the LREE. They argued that the extent of melting was sufficiently low, such that it did not lead to a resolvable fractionation of Re or Pt from Os. The modelling was based on the assumption that partitioning behaviour of Re during mantle melting was similar to that of Yb (Righter and Hauri, 1998). More recent studies, however, have suggested that the incompatibility of Re increases dramatically with increasing oxygen fugacity, and that at oxygen fugacities typical of melting leading to formation of, for example, MORB, Re partitioning behaviour is more similar to that of Ti (Mallmann and O'Neill, 2007). If this is the case, the differing degree of depletion recorded by the Sm–Nd and Re–Os isotope systematics in the mantle may not be adequately explained by the differing behaviour during the same process and may, thus, have a different origin.

To examine these issues in greater detail, we obtained Sm–Nd and Pt–Re–Os isotopic and REE and HSE abundance data for Tony's flow, a differentiated komatiite lava flow from the 2.7 Ga Belingwe greenstone belt in Zimbabwe. We also report additional Pt–Re–Os isotopic and HSE abundance data for the PH-II flow from Munro Township in the 2.7 Ga Abitibi greenstone belt, Canada, which extend the data from the Puchtel et al. (2004a) study. These two komatiites are particularly interesting to compare because they are approximately of the same age, geochemically similar, yet presumably formed far apart.

2. GEOLOGICAL BACKGROUND, SAMPLES, AND PREVIOUS STUDIES

2.1. Belingwe greenstone belt

The upper part of the Belingwe Greenstone Belt (BGB) consists of the Ngezi Group, an ~8 km thick volcanic and

sedimentary sequence which lies unconformably upon older greenstones, and in part upon the 3.5–3.6 Ga Shabani Greiss Complex (Bickle et al., 1975; Nisbet et al., 1993b). The lowermost unit of the Ngezi Group is the 0–100 m thick Manjeri Formation, consisting of shallow-water clastic sediments, carbonates, and ironstones. It is conformably overlain by the ~1 km thick Reliance Formation containing mafic and ultramafic volcanic and volcaniclastic lithologies. The rocks analyzed in this study come from the part of the Ngezi Group that overlies the ancient Shabani gneisses. Overlying the Reliance Formation is the dominantly basaltic, up to 5 km thick, Zeederbergs Formation, which is, in turn, succeeded by the shallow-water sediments of the up to 2 km thick Cheshire Formation (Bickle et al., 1975; Nisbet et al., 1977). Komatiites are confined to the Reliance Formation, which consists of three main units (Nisbet et al., 1977). The lower (up to 400 m thick) and upper (up to 200 m thick) members contain primarily komatiitic basalts and tuffs, whereas the middle member (400 m thick) consists of a series of komatiite lava flows. A komatiite lava flow from the center of the Reliance Formation, the Tony's flow, referred to hereafter as the TN flow, has been selected for this study (Fig. 1). This flow has been sampled in a surface outcrop and later intersected by the core of the SASKMAR drill hole. The results of the field and petrographic studies were reported by Nisbet et al. (1987) and Renner et al. (1994). The TN flow is completely exposed in surface outcrop that is well correlated with the drill site area. The flow is extremely well preserved, commonly with unaltered primary mineralogy and even pristine glass remaining within olivine grains. The flow differentiated into an upper spinifex (A) zone and a lower cumulate (B) zone. The porphyritic $B_{2\text{-}4}$ subzones consist of up to 50% of solid equant olivine microphenocrysts $Fo_{91.3}$ that comprise >95% of the cumulate grain population, and larger equant olivine grains up to Fo_{94} that comprise <5% of the cumulate grain population; the latter have been interpreted to be xenocrysts.

Nisbet et al. (1987) and Bickle et al. (1993) published first lithophile trace element and Nd, Sr, and O isotopic data for komatiites from the Reliance Formation, and variations of some PGE abundances in the Anderson's and Onias's flows were studied by Zhou (1994). Walker and Nisbet (2002) reported Re–Os isotopic data for samples from the Tony's and Onias's flows. Chauvel et al. (1993) obtained a precise Pb–Pb isochron age of 2692 ± 9 Ma for komatiitic basalts from the Reliance Formation, which was interpreted to reflect the emplacement age of the supracrustal sequences.

For the present study, we analyzed 9 surface outcrop (ZV) and 23 drill core (TN) samples from Tony's flow (Fig. 1). The surface outcrop samples we used in this study are large hand specimens, parts of which were used in the Nisbet et al. (1987) and Renner et al. (1994) studies, whereas the drill core samples that we studied have so far not been analyzed.

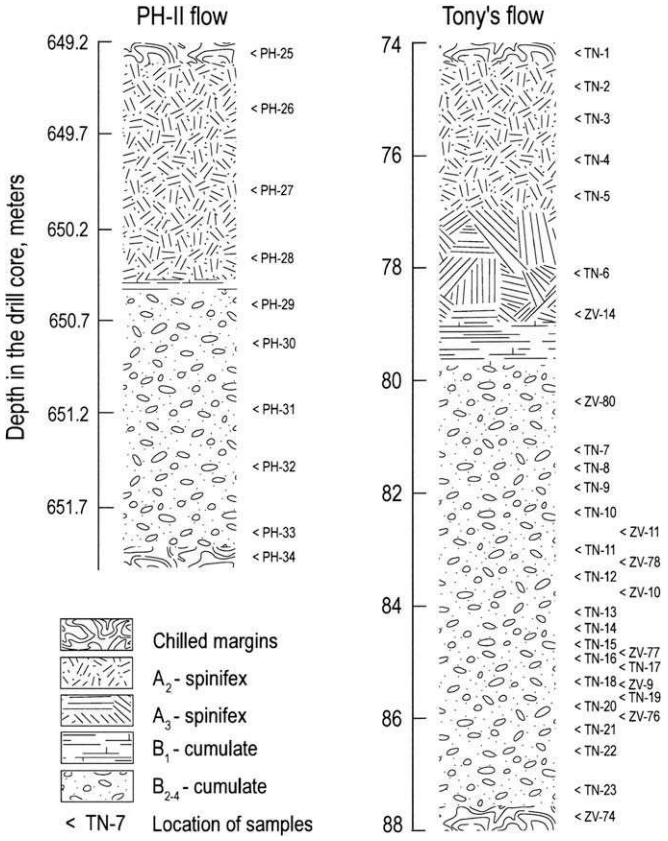

Fig. 1. Schematic sections through the TN and PH flows and location of samples analyzed in this study.

2.2. Abitibi greenstone belt

The geology of the Abitibi Greenstone Belt (AGB) and field petrology of mafic and ultramafic lavas from the Pyke Hill area have been described in detail in a number of publications (e.g., Pyke et al., 1973; Arndt et al., 1977; Sproule et al., 2002, 2005). Most of the stratigraphic, geochronological, and geochemical evidence favors a predominantly autochthonous model for the AGB (Sproule et al., 2002). The latter has been subdivided into several lithotectonic assemblages ranging in age between 2750 and 2703 Ma based on the high-precision U–Pb zircon data (Ayer et al., 2002). The Pyke Hill area belongs to the Kidd–Munro Assemblage, which, in addition to komatiites (~5% of the total assemblage), also contains mafic, intermediate, and felsic volcanic rocks and iron formations (Ayer et al., 2002). The U–Pb zircon ages of felsic lavas that underlie and overlie the komatiites are 2715 ± 2 and 2703 ± 2 Ma, respectively (Ayer et al., 2002).

Regression of the available Sm–Nd data for the Kidd–Munro Assemblage komatiites compiled by Puchtel et al. (2004b) from the studies of Dupré et al. (1984), Walker et al. (1988), and Lahaye and Arndt (1996) and corrected for the instrumental bias between different laboratories yielded an age of 2713 ± 29 Ma and an initial $\varepsilon^{143}Nd = +2.9 \pm 0.2$. The first terrestrial Re–Os isochron was obtained by Walker et al. (1988) for komatiites from the Pyke Hill area. The age of 2726 ± 93 Ma defined by the isochron was consistent with the emplacement age of the lavas, and the initial Os isotopic composition derived from the isochron indicated that the mantle source of the Pyke Hill komatiites evolved with time-integrated near-chondritic Re/Os. Gangopadhyay and Walker (2003) reported a Re–Os isochron age of 2762 ± 76 Ma and also a roughly chondritic initial $\gamma^{187}Os = -0.1 \pm 1.0$ for a set of whole-rock samples and chromite separates from a surface flow in the nearby Alexo area. Gangopadhyay et al. (2005) also obtained an initial $\gamma^{187}Os = 0.0 \pm 0.6$ for a series of whole-rock samples and chromite separates from the Dundonald Beach area, also within the Kidd–Munro Assemblage.

The major, minor, and lithophile trace element data for komatiite lavas from the Munro Township area have been reported by Arndt et al. (1977) and Sproule et al. (2002) and, more recently, for the samples used in this study, by Puchtel et al. (2004a,b).

A 2.7-m thick differentiated komatiite lava flow, the PH-II flow from Puchtel et al. (2004a,b), further referred to as the PH flow, has been selected for this study (Fig. 1). Details of the mineralogical and textural features of the PH flow, given in Puchtel et al., (2004b), are very similar to those described by Pyke et al. (1973) and also to those of the TN flow. The PH flow is also subdivided into an upper spinifex (A) and a lower cumulate (B) zones. Almost all olivine is altered to serpentine, chlorite, and magnetite, although chromite is well preserved. The composition of solid equant olivine grains from the B_2 subzone varies in a narrow range between $Fo_{93.5–94.4}$, with up to 52.6% MgO (Puchtel et al., 2004b).

In this study, using sample powder aliquots from Puchtel et al. (2004a), we obtained more precise age and the source HSE composition for the Pyke Hill komatiites by analyzing additional samples, including those with higher Re/Os and Pt/Os ratios. In order to make the results obtained in the two laboratories more comparable, we also replicated several samples analyzed by Puchtel et al. (2004a).

3. ANALYTICAL TECHNIQUES

3.1. Sample preparation and mineral separation

The TN samples were processed using the same protocol utilized in the study of the Abitibi komatiites (Puchtel et al., 2004b). Each drill core sample, 400–600 g in weight, where necessary, was split in quarters lengthwise using a diamond saw, and one quarter was used for the chemical studies. The quarters were hand-polished on all sides using SiC sandpaper to remove drill bit or saw marks, washed in Milli-Q water, dried, and crushed in an alumina-faced jaw crusher. A 100-g aliquot of crushed sample was ground in an alumina shatter box and then finely re-ground in an alumina-faced disk mill. From the hand specimens, 200–400 g slabs were cut using a diamond saw for mineral separation and chemical studies. After removing any signs of weathering using the diamond saw, these slabs were processed using the same protocol applied to the drill core samples. The crush of the largest (500 g) and freshest hand specimen, ZV10, was used for mineral separation; olivine and chromite separates were obtained at the Institute of Geology in Petrozavodsk using the combination of heavy liquid and magnetic separation techniques and handpicking.

3.2. Major and minor elements

Major and minor element analyses were carried out at the Franklin & Marshall College on fused glass discs using a Phillips 2404 XRF vacuum spectrometer equipped with a 4 kW Rh X-ray tube, following the protocol of Mertzman (2000). The typical accuracy of the analyses was ~1% relative for major elements present in concentrations >0.5% and ~5% relative for the rest of major and for minor elements. The details of major and minor element analysis techniques for the PH flow were reported by Puchtel et al. (2004b).

3.3. REE abundances and Sm–Nd isotopic systematics

The REE abundances in the TN and PH flows were determined at the Institute of Mineralogy and Geochemistry of Trace Elements in Moscow. Mixed REE spike, 50–100 mg sample powder, and 1–2 mL of double-distilled concentrated HF, HNO_3, and $HClO_4$. were sealed in Teflon digestion vessels and equilibrated in a Multiwave® microwave oven at 260 °C for ~3 h. After digestion, the sample solutions were dried, the residues were converted into the chloride form, and REE were first separated from the silicate matrix, and then further purified using cation exchange chromatography. The samples were run on a Perkin Elmer ELAN 6100 DRC ICP-MS. The accuracy of the analyses

was estimated to be ~2% (relative) for all elements and was determined by multiple analyses of the USGS standards BCR, BHVO, and BIR.

For the Sm–Nd isotopic analyses of the TN flow, ~200 mg of sample powder, 1 mL of conc. HF, 3 mL of conc. HNO_3 (all double-distilled), and appropriate amounts of a mixed ^{149}Sm–^{150}Nd spike were weighted out into screw-cap 15 mL Teflon vessels, sealed and digested on a hotplate at 140 °C for 24 h. The vessels were then opened, the solutions were dried, new portions of acids were added, and the digestion procedure was repeated for another 24 h. The REE were first separated from the silicate matrix using cation exchange chromatography, and then the Nd and Sm fractions were separated and purified using Eichrom Ln resin. The Nd and Sm cuts were run in a static mode using Faraday cups of the *Nu Plasma* ICP-MS at the *Isotope Geochemistry Laboratory*, University of Maryland College Park *(IGL)*. The effects of mass-fractionation during Nd runs were corrected for by normalizing to $^{146}Nd/^{144}Nd = 0.7219$. Measurements of a 200 ppb Nd La Jolla standard solution during the period of data collection yielded $^{143}Nd/^{144}Nd = 0.511873 \pm 15$ ($2\sigma_{stdev}$; $N = 4$). The measured $^{143}Nd/^{144}Nd$ ratios in the samples were bias-corrected to the La Jolla $^{143}Nd/^{144}Nd = 0.511860$. The initial $\varepsilon^{143}Nd$ values were calculated based on the present-day parameters of the chondrite uniform reservoir (CHUR): $^{147}Sm/^{144}Nd = 0.1967$ (Jacobsen and Wasserburg, 1980), $^{143}Nd/^{144}Nd = 0.512638$ (Hamilton et al., 1983).

3.4. Highly siderophile elements

The details of the analytical protocol used in the HSE analysis are given in Puchtel et al. (2004a), Puchtel et al. (2005) and Puchtel et al. (2007) and are only briefly summarized below.

3.4.1. Re–Os isotopic systematics and HSE abundances

Approximately 1.5 g of whole-rock sample powder, 2.0 g of pure olivine, or 0.075 g of pure chromite separate, 6 mL of purged, triple-distilled conc. HNO_3, 4 mL of triple-distilled conc. HCl, and appropriate amounts of mixed ^{185}Re–^{190}Os and HSE (^{99}Ru,^{105}Pd,^{191}Ir,^{194}Pt) spikes were sealed in double internally-cleaned, chilled 25 mL Pyrex™ borosilicate Carius Tubes (CTs) and heated to 270 °C for 96 h. Osmium was extracted from the acid solution by CCl_4 solvent extraction (Cohen and Waters, 1996), then back-extracted into HBr, followed by purification via microdistillation (Birck et al., 1997). Ru, Pd, Re, Ir, and Pt were separated and purified using anion exchange chromatography. Average total analytical blanks during the analytical campaign were (pg): Ru 0.50 ± 0.16 ($\pm 2\sigma_{mean}$, $N = 14$), Pd 13 ± 7, Re 1.1 ± 0.3, Os 0.25 ± 0.11, Ir 0.29 ± 0.07, and Pt 18 ± 7. For Os, Ir, Ru, and Pd, the blanks, on average, constitute less than 0.1%, and for Re and Pt, less than 0.2% of the total element analyzed, respectively. The exceptions were the chromite and olivine separates, for which blank contributions for Re were 2.4% and 16%, for Pt 6% and 5%, and for Pd 0.8% and 4%, respectively.

Osmium isotopic measurements were accomplished via negative thermal ionization mass-spectrometry (NTIMS: Creaser et al., 1991). All samples were analyzed using a secondary electron multiplier (SEM) detector of the VG *Sector 54* mass spectrometer at the *IGL*. Each Os load was run two times for a total data collection time of ~12 h. The data from the two runs for each sample were averaged and reported as the final result. The measured isotopic ratios were corrected for mass-fractionation using $^{192}Os/^{188}Os = 3.083$. The $^{187}Os/^{188}Os$ in 300 pg loads of the Johnson–Matthey Os standard measured repeatedly during the analytical campaign averaged 0.11360 ± 22 ($\pm 2\sigma_{stdev}$, $N = 21$). This value characterizes the external precision of the isotopic analysis (0.2%) and was used to calculate the uncertainty on the measured Os isotopic composition for each individual sample. The $^{187}Os/^{188}Os$ ratio measured in each sample was corrected for the instrumental bias relative to the average $^{187}Os/^{188}Os = 0.11378$ measured in the Johnson–Matthey Os standard on the Faraday cups of the *IGL Triton*. The correction factor of 1.00158 was calculated by dividing this value by the average $^{187}Os/^{188}Os$ measured in the Johnson–Matthey Os standard on the SEM of the *IGL Sector 54* instrument.

The measurements of Ru, Pd, Re, Ir, and Pt were performed at the *IGL* by inductively coupled plasma mass-spectrometry (ICP-MS) using a *Nu Plasma* instrument with a triple electron multiplier configuration in a static mode. Isotopic mass-fractionation was corrected for by interspersal of samples with standards. The accuracy of the data was assessed by comparing the results for the reference materials UB-N and GP-13, obtained during the ongoing analytical campaign, with the results from other laboratories. Concentrations of all HSE and Os isotopic compositions obtained at the *IGL* are in good agreement with the other labs (Puchtel et al., 2007, 2008). Diluted spiked aliquots of iron meteorite samples were run during each analytical session as secondary standards. The results from these runs agreed within 0.5% for Ir, 0.8% for Re, and 2% for Ru, Pt, and Pd with fractionation-corrected values obtained from measurements of undiluted iron meteorite samples using Faraday cups of the same instrument with a signal of >100 mV for the minor isotopes. We therefore cite ±2% as uncertainty on the concentrations of Ru, Pt, and Pd, ±0.8% for Re, ±0.5% for Ir, and ±0.2% for the concentrations of Os in the whole-rock samples. For the chromite and olivine separates, the uncertainties on the Re concentrations were 1.2% and 8%, Pt – 3% and 2.5%, and Pd – 0.4% and 2%, respectively, assuming a ~50% variation in abundances in the blank. The uncertainty in the Re concentration was the main source of uncertainty in the Re/Os ratio. This uncertainty was, thus, estimated to be 0.8% for the whole-rock samples, 1.2% for the chromite, and 8% for the olivine separates. All regression calculations were performed using ISOPLOT 3.00 (Ludwig, 2003) and the uncertainties stated above. The initial $\gamma^{187}Os$ value was calculated as the per cent deviation of the isotopic composition at the time defined by the isochron relative to the chondritic reference of Shirey and Walker (1998) at that time. The average chondritic Os isotopic composition at the time T defined by the isochron was calculated using the ^{187}Re decay constant $\lambda = 1.666 \times 10^{-11}$ year^{-1}, an early solar system $^{187}Os/^{188}Os = 0.09531$, and the present-day

average chondritic composition ($^{187}Re/^{188}Os = 0.40186$, $^{187}Os/^{188}Os = 0.1270$: Smoliar et al., 1996; Shirey and Walker, 1998).

3.4.2. Pt–Os isotopic systematics

In the present study, we followed the methodology developed by Puchtel et al. (2004a) for determining precise initial $^{186}Os/^{188}Os$ isotopic compositions in materials requiring corrections for the ingrowth of radiogenic ^{186}Os, such as Archean komatiites. This methodology involves determination of high precision $^{186}Os/^{188}Os$ isotopic compositions on un-spiked digestions combined with determination of elemental abundance ratios of Pt, Re, and Os on small aliquots taken from the un-spiked digestions to ensure the representativeness of these ratios for each sample digestion. In order to obtain the amount of Os required for the high-precision measurements of the $^{186}Os/^{188}Os$ and $^{187}Os/^{188}Os$ ratios (50–70 ng), each sample was digested in 8–16 CTs. For the initial un-spiked digestions, ~3 g of sample powder and 15 mL of acids were placed into 37 mL Pyrex™ CTs, chilled to 0 °C, sealed and kept in an oven at ~270 °C for 96 h. After the digestion was complete, the tubes were chilled and opened, 0.5 mL of the acid sample solution from each CT of the batch representing a single sample digestion were transferred into a clean 25 mL CT for precise determination of the Re/Os and Pt/Os ratio in each sample. Before the transfer procedure, the clean CT was chilled to 0 °C and appropriate amounts of the mixed ^{185}Re–^{190}Os and HSE (^{99}Ru, ^{105}Pd, ^{191}Ir, ^{194}Pt) spikes were added to it, followed by ~5 mL of acid after the sample solution transfer was completed. The CT with the spiked sample solution was then sealed and kept in an oven at ~270 °C for 24 h to achieve sample-spike equilibration. After opening the CT, the spiked aliquot was processed using the same procedure utilized in the Re–Os and HSE analysis, except that, without a knowledge of the precise weight of the sample represented by the amount of transferred solution, only the inter-element ratios of interest directly pertaining to the scope of this part of the study (i.e., Re/Os and Pt/Os) were determined. From the remaining part of the un-spiked acid sample solution, Os was extracted and purified using the same protocol utilized in the Re–Os study. The Os cuts from the batch of CTs containing a single sample digestion were combined into one cut and used for the precise measurements of the $^{186}Os/^{188}Os$ and $^{187}Os/^{188}Os$ ratios.

Measurements of Re, Os, and Pt isotopic compositions from the spiked aliquots, for the determination of precise Re/Os and Pt/Os ratios, were performed using the same protocol utilized in the Re–Os and HSE study outlined above.

The high-precision measurements of the $^{186}Os/^{188}Os$ and $^{187}Os/^{188}Os$ ratios were performed by *N-TIMS* in a static mode on either a nine-Faraday collector *ThermoFinnigan Triton®* mass spectrometer at the NASA Johnson Space Center (*JSC*), or on a nine-Faraday collector *Triton®* mass spectrometer at the *IGL*. Signals of 100–180 mV on mass 234 ($^{186}Os^{16}O_3^-$) and 235 ($^{187}Os^{16}O_3^-$) were generated to reach the maximum in-run precisions. The possible isobaric interference of $^{186}W^{16}O_3^-$ on $^{186}Os^{16}O_3^-$ was assessed by measuring $^{184}Os/^{188}Os$ (modified if $^{184}W^{16}O_3^-$ present) and monitoring mass 231 ($^{183}W^{16}O_3^-$). Although a signal of ~50 cps was normally measured at mass 231, its size in comparison to other potential isotopes of W indicated it was not W, and, therefore, no W corrections were made. Instead, the small signals typically observed at mass 231 are consistent with the expected amount of $^{198}Pt^{16}O^{17}O$ that is produced from the Pt filaments during ionization. This was indicated from the mass scan profiles from mass 226 ($^{194}Pt^{16}O_2$) to mass 230 ($^{198}Pt^{16}O_2$), that clearly show all of the PtO_2 isotopes in their expected proportions in the spectrum, and no evidence for WO_3 production at mass 230 or 231. The mean of the Johnson–Matthey Os standard runs during the period of data collection was 0.0013071 ± 54 and 0.0013086 ± 57 for $^{184}Os/^{188}Os$, 0.1198475 ± 11 and 0.1198454 ± 17 for $^{186}Os/^{188}Os$, and 0.1137921 ± 42 and 0.1137840 ± 48 for $^{187}Os/^{188}Os$ ($2\sigma_{stdev}$) at the *JSC* ($N = 6$) and at the *IGL* ($N = 16$), respectively. The measured $^{186}Os/^{188}Os$ at the *IGL* were bias-corrected to the *JSC* $^{186}Os/^{188}Os$ standard value of 0.1198475 using a correction coefficient of 1.0000175. Each sample load was run two to four times; the reported results represent averages of all individual runs, and the errors on the averages are quoted at $2\sigma_{mean}$. To calculate the age, the Pt–Os data were regressed using ISOPLOT 3.00 and the ^{190}Pt decay constant $\lambda = 1.477 \times 10^{-12}$ year^{-1} (Begemann et al., 2001). Error input was determined from either the uncertainty of the standard measurements, or the uncertainty of the individual runs, whichever was greater. All errors on age and initial isotopic ratios are quoted at $2\sigma_{mean}$. The initial $\varepsilon^{186}Os$ values were calculated as part per 10,000 deviation of the $^{186}Os/^{188}Os$ of the sample at the time relative to the chondritic reference of Brandon et al. (2006) at that time using an early solar system $^{186}Os/^{188}Os = 0.1198269$ and $^{190}Pt/^{188}Os = 0.00174$.

4. RESULTS

4.1. Major, minor and trace elements in the emplaced komatiite lavas

The major, minor, and REE data for the TN and PH flows are presented in Tables 1 and 2 and plotted on variation diagrams in Fig. 2. The primitive mantle-normalized REE abundances in the lavas are also plotted in Fig. 3. The concentrations in both flows vary in a manner typical of differentiated komatiite lava flows elsewhere (e.g., Arndt, 1986). In the TN flow, the upper chilled margin contains 24% MgO, compared to 28% in the PH flow. In the TN flow, the MgO content ranges between 24% and 17% in the A-zone and between 26% and 31% in the B-zone, compared to 28–27% and 27–35%, respectively, in the PH flow. The PH flow is, therefore, somewhat more MgO-rich, and exhibits a narrower range in the MgO content, likely due to the fact that it is a thinner flow. Both compatible and incompatible elements in the TN and PH flows vary in a regular fashion. When plotted against MgO, the data for incompatible Al_2O_3, TiO_2, CaO (TN only), V, and REE define tight trends with negative slopes intersecting the MgO axes at $50.2 \pm 0.5\%$ and $52.6 \pm 0.7\%$ ($2\sigma_{mean}$) for the TN

Table 1
Major (wt.%) and minor (ppm) element data for the TN flow.

Sample	SiO_2	TiO_2	Al_2O_3	Fe_2O_3	MnO	MgO	CaO	Na_2O	K_2O	P_2O_5	LOI	Cr	V	Co	Ni
TN1	46.9	0.366	7.29	12.7	0.215	24.0	7.22	0.54	0.140	0.022	6.61	2332	156	97	1391
TN2	48.1	0.410	8.08	12.9	0.210	20.2	8.48	1.05	0.095	0.021	4.18	2367	179	83	985
TN3	48.3	0.419	8.27	13.1	0.220	20.3	7.86	0.97	0.084	0.021	3.85	2455	183	79	1006
TN4	47.6	0.384	7.77	12.9	0.208	21.6	7.85	1.05	0.052	0.021	2.98	2383	174	77	1254
TN5	48.4	0.417	8.26	13.1	0.209	19.5	8.48	1.12	0.073	0.021	3.30	2369	184	82	880
TN6	48.6	0.436	8.76	13.4	0.218	18.1	8.58	1.25	0.083	0.021	2.95	2191	188	84	758
ZV14	49.4	0.463	9.28	13.4	0.216	16.5	9.02	1.16	0.062	0.021	2.79	2024	203	74	541
ZV80	46.3	0.310	6.23	12.4	0.165	26.7	6.44	0.70	0.010	0.010	2.69	2286	138	90	1788
TN7	45.7	0.311	6.15	12.1	0.197	27.8	6.26	0.80	0.021	0.021	2.81	2287	136	90	1823
TN8	45.5	0.300	5.99	12.2	0.197	28.3	6.03	0.77	0.021	0.010	2.56	2336	132	106	1822
TN9	45.8	0.299	5.96	12.1	0.196	28.3	6.01	0.78	0.021	0.021	2.47	2269	129	99	1802
TN10	45.5	0.304	5.77	12.1	0.199	28.8	6.04	0.65	0.010	0.010	3.75	2260	130	99	1901
ZV11	46.2	0.310	6.11	12.2	0.196	27.7	6.01	0.60	0.021	0.010	2.86	2258	135	98	1889
TN11	45.4	0.290	5.78	11.9	0.196	29.1	5.83	0.78	0.010	0.021	2.40	2227	126	86	1784
ZV78	46.1	0.312	6.07	12.3	0.198	27.9	5.89	0.56	0.021	0.010	3.63	2329	141	109	1812
TN12	45.3	0.280	5.54	11.9	0.187	29.8	5.61	0.66	0.021	0.010	3.03	2287	124	103	2003
ZV10	46.2	0.308	6.19	12.2	0.195	27.5	6.11	0.66	0.021	0.021	2.16	2284	137	108	1804
TN13	45.5	0.279	5.46	11.8	0.186	30.1	5.43	0.67	0.021	0.010	2.59	2237	123	104	1998
TN14	45.4	0.270	5.41	11.8	0.187	30.2	5.45	0.63	0.021	0.010	2.88	2221	122	100	2141
TN15	45.3	0.268	5.35	11.8	0.186	30.4	5.43	0.62	0.021	0.010	2.18	2226	123	108	2068
ZV77	46.5	0.318	6.33	12.3	0.195	26.6	6.39	0.75	0.021	0.021	2.10	2247	143	93	1782
TN16	45.0	0.259	5.18	11.9	0.186	31.0	5.21	0.61	0.010	0.010	3.07	2247	116	114	2245
TN17	44.7	0.261	5.05	11.9	0.188	31.3	5.35	0.58	0.021	0.010	3.95	2276	113	102	2209
TN18	45.2	0.262	5.27	11.9	0.189	30.4	5.50	0.64	0.021	0.010	4.35	2244	123	114	2320
ZV9	46.0	0.310	6.04	12.3	0.197	27.5	6.15	0.80	0.031	0.010	2.76	2304	136	109	1883
TN19	45.3	0.279	5.32	11.8	0.186	30.3	5.48	0.63	0.010	0.010	2.68	2223	122	96	2131
TN20	45.5	0.278	5.43	11.7	0.195	29.9	5.49	0.77	0.021	0.010	2.25	2234	124	105	2093
ZV76	46.3	0.319	6.31	12.4	0.196	26.7	6.37	0.84	0.021	0.021	2.52	2248	140	98	1765
TN21	45.5	0.283	5.62	12.0	0.189	29.6	5.51	0.55	0.021	0.021	4.27	2267	126	99	2033
TN22	45.8	0.303	5.83	12.1	0.198	28.8	5.83	0.51	0.010	0.021	3.56	2226	129	97	1972
TN23	46.7	0.313	6.19	12.3	0.198	27.8	5.25	0.63	0.021	0.010	3.37	2226	133	100	1857
ZV74	46.3	0.330	6.56	12.4	0.196	26.1	6.57	0.87	0.041	0.021	2.31	2279	143	99	1668

Note. The analyses are re-calculated on an anhydrous basis.

Table 2
REE (ppm) data for the Tony's flow.

Sample	Ce	Nd	Sm	Eu	Gd	Dy	Er	Yb	$(Ce/Sm)_N$	$(Gd/Yb)_N$
TN1	2.02	1.93	0.710	0.301	1.11	1.39	0.906	0.881	0.69	1.02
TN3	2.37	2.27	0.831	0.332	1.27	1.54	1.05	1.02	0.69	1.01
TN4	2.18	2.06	0.782	0.329	1.19	1.53	0.979	0.963	0.67	1.00
TN6	2.57	2.38	0.912	0.367	1.36	1.72	1.13	1.05	0.68	1.05
ZV14	2.77	2.57	0.950	0.397	1.44	1.79	1.18	1.13	0.70	1.03
ZV10	1.80	1.67	0.613	0.250	0.969	1.18	0.795	0.761	0.71	1.03
TN16	1.50	1.42	0.543	0.213	0.784	1.02	0.674	0.644	0.66	0.98
TN19	1.54	1.49	0.558	0.227	0.822	1.02	0.667	0.665	0.67	1.00

Note. Normalizing values (N) are from Hofmann (1988). The analyses are re-calculated on an anhydrous basis.

and PH flows, respectively. These projected MgO abundances are consistent with the average MgO contents of cores of olivine microphenocrysts crystallized in the B zones of the TN ($50.8 \pm 0.6\%$: Renner et al., 1994) and PH ($51.6 \pm 0.2\%$: Puchtel et al., 2004b) flows and, thus, indicate that the trends for these elements represent olivine control lines, also testifying to the immobile behaviour of these components. The CaO data for the PH flow plot on a steeper trend that does not pass through the olivine composition but, instead, intersects the MgO axis at $42.9 \pm 1.9\%$. This implies CaO mobility during alteration of the PH flow, most likely the olivine-rich, cumulate portion of it, on the scale of drill core samples.

The Ni vs. MgO data for both flows define trends with positive slopes indicating the typical compatible behaviour of Ni during lava differentiation. However, although the PH flow trend passes near the cumulate olivine composition, indicating olivine control over the variations of this element, the TN trend has a slightly steeper slope than the olivine control line, as defined by the average Ni content

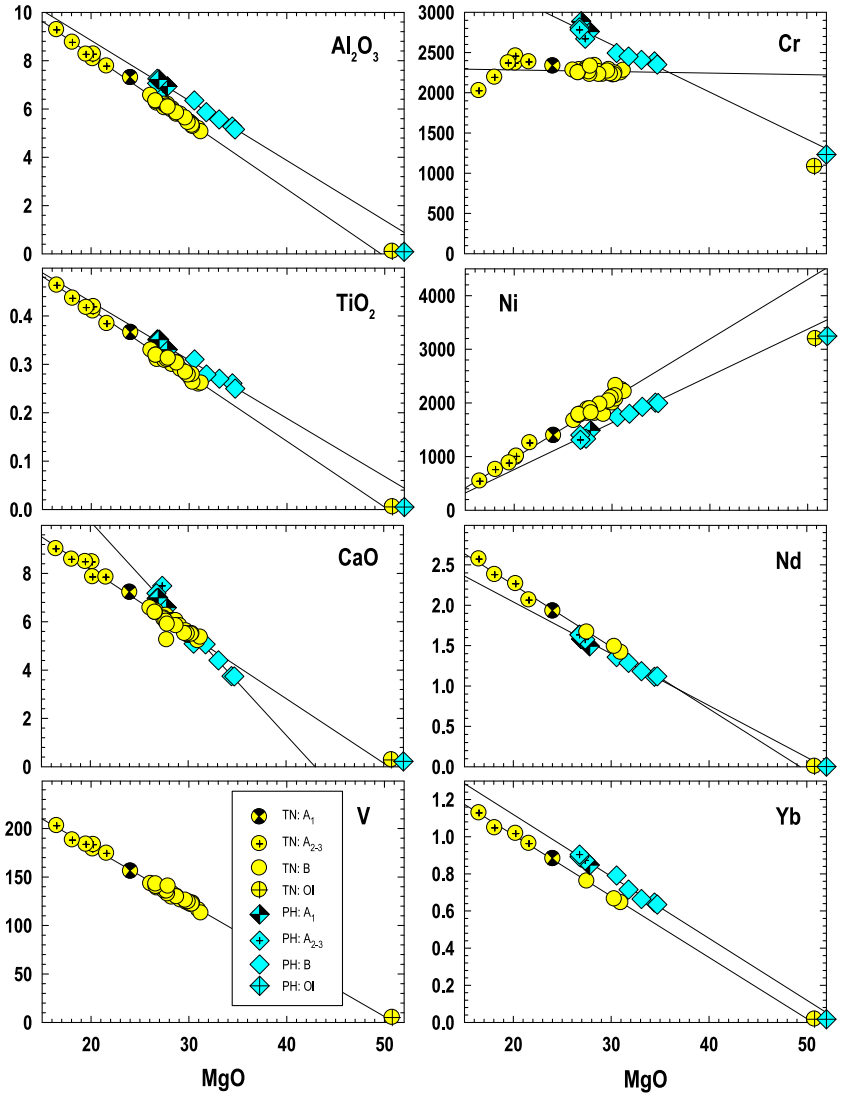

Fig. 2. Variations of selected major, minor, and trace element abundances in whole-rock komatiite samples and olivine separates from the TN and PH flows. Except for the MgO, Ni, CaO, and Cr contents, which are from Renner et al. (1994), the abundances in the olivine separates were calculated using the composition of the emplaced lava and the olivine-silicate melt partition coefficients of Green (1994).

in the cumulus olivine, and may indicate the presence of a minor Ni-rich phase on the liquidus, in addition to olivine. The Cr data for most samples from the TN flow plot on an essentially horizontal trend that passes well above the cumulate olivine composition. In addition, samples from the spinifex zone exhibit a distinct positive correlation of Cr vs. MgO. These relationships indicate fractionation of minor chromite in the TN flow. In contrast, the Cr data for the entire PH flow plot on a trend that passes through the cumulate olivine composition, indicating that Cr variations in the flow were controlled solely by olivine fractionation.

The average primitive mantle (PM)-normalized (Hofmann, 1988) Al_2O_3/TiO_2 and Gd/Yb are 0.88 ± 0.01 and 1.01 ± 0.02 (TN) and 0.92 ± 0.01 and 0.96 ± 0.01 (PH), respectively ($2\sigma_{mean}$). These values are consistent with the composition of the komatiite type that was classified by Nesbitt and Sun (1976) as Al-undepleted, or Munro-type lavas. The PM-normalized CaO/Al_2O_3 in the TN flow and in the presumably alteration-free A-zone of the PH flow are 1.27 ± 0.02 and 1.26 ± 0.07, respectively, i.e., these ratios are ~30% higher than that in the PM. Finally, both flows are depleted in LREE relative to PM (Fig. 3), with average $(Ce/Sm)_N = 0.68 \pm 0.01$ (TN) and 0.52 ± 0.01 (PH).

Accurate determination of the MgO contents of the emplaced komatiite lavas is important for evaluating the potential mantle temperature of magma generation, and, ultimately, for calculating the absolute and relative lithophile and HSE abundances in their mantle sources. We used several independent techniques to calculate the MgO contents of the emplaced komatiite lavas for the TN and PH flows. First, we used the compositions of upper chilled margins that are usually good proxies for the liquid composition from which they formed. These are represented by samples TN1 and PH25, which contain 24.0% and 27.8%

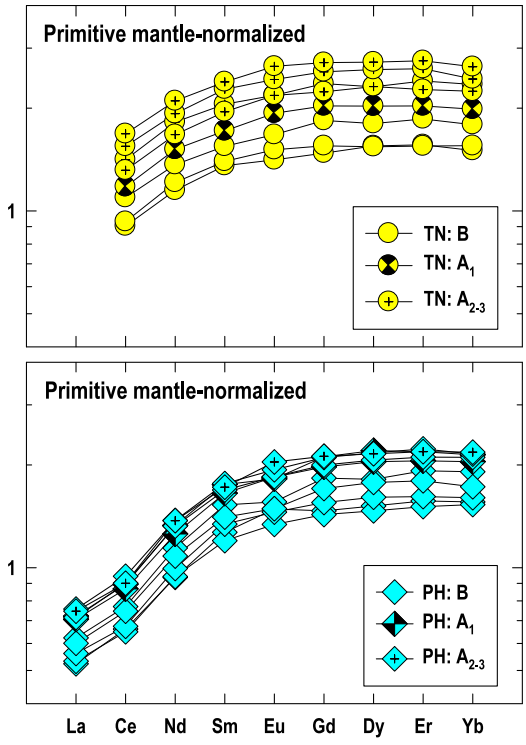

Fig. 3. Primitive mantle-normalized (Hofmann, 1988) REE abundances in the TN and PH flows.

MgO, respectively. Second, we used a well-established relationship between the composition of cumulate olivine and that of the liquid it crystallized from (Roeder and Emslie, 1970; Beattie et al., 1991). The average MgO and FeO contents of the cores of olivine microphenocrysts (not xenocrysts, which were not included into the calculations) in the TN flow are $50.8 \pm 0.6\%$ and $7.7 \pm 0.8\%$ ($2\sigma_{mean}$), as compiled from Renner et al. (1994). These olivine compositions can be shown to be in equilibrium with a komatiite liquid containing $24.7 \pm 2.1\%$ MgO. In the PH flow, the average MgO and FeO contents of the cores of olivine phenocrysts are $51.6 \pm 0.2\%$ and $6.3 \pm 0.2\%$ ($2\sigma_{mean}$), respectively; these olivines can be shown to be in equilibrium with a komatiite liquid containing $27.0 \pm 1.0\%$ MgO. Finally, we extrapolated the differentiation trends for the elements that are absent from olivine crystal lattice towards their intercepts with the MgO axis to calculate the average MgO content of olivine that crystallized from the emplaced lava. We then used this composition to calculate the MgO content of the emplaced lava from the relationship between the composition of the olivine and the liquid it crystallized from. The linear regressions give average intercept values of 50.2 ± 0.5 and $52.6 \pm 0.7\%$ for the average MgO content in the olivine from the TN and PH flows, respectively, which are calculated to be in equilibrium with komatiite liquid containing $24.8 \pm 2.3\%$ (TN) and $29.0 \pm 2.5\%$ MgO (PH). The average MgO contents in the emplaced lavas are, thus, calculated to be $24.5 \pm 0.5\%$ and $27.9 \pm 1.2\%$ for the TN and PH flows, respectively ($2\sigma_{mean}$). Our results for the TN flow are consistent with those of Nisbet et al. (1993a) who concluded that the most MgO-rich erupted komatiitic liquids known from the Reliance Formation contained ~26% MgO.

4.2. HSE abundance data and HSE composition of the emplaced komatiite lava

The HSE abundances obtained in this study for the TN and PH flows are presented in Table 3 and plotted as CI chondrite-normalized (using average Orgueil values from Horan et al., 2003) abundances in Fig. 4. These new HSE data together with those from the Puchtel et al. (2004b) study are also plotted against MgO contents in Fig. 5.

The olivine and chromite separates from the TN flow exhibit similar CI chondrite-normalized patterns with enrichments in IPGE (IPGE = Os, Ir, and Ru: Barnes et al., 1985), especially Ru, relative to PPGE (PPGE = Pt and Pd) and Re, albeit the chromite has about an order of magnitude higher Os, Ir, and Pt and about two orders of magnitude higher Ru, Pd, and Re contents compared to the olivine. The similarities in the pattern shape between the olivine and chromite may suggest that the HSE budget of the olivine may be in part controlled by the presence of micron-sized chromite inclusions that are observed in thin sections.

In whole-rock samples of both lava flows, all HSE show strong correlations with the indices of magmatic differentiation, such as MgO contents, which is evidence for their immobile behaviour during post-magmatic processes. Os and Ir strongly, positively correlate with the MgO content, which indicates compatible behaviour of these elements during lava differentiation. This is typical of the so-called Munro-type lava flows of Puchtel and Humayun (2005). The olivine compositions plot well below the trends for either flow, indicating the presence of an Os and Ir-rich phase on the liquidus. Because of the minimal variance (e.g., Figs. 4 and 5), it appears that the bulk differentiation partition coefficients for Ru were close to unity for both flows, with the Ru concentrations across the lava flows being mostly controlled by olivine, possibly with a small proportion of chromite in the case of the TN flow. Re, Pt, and Pd display negative linear correlations with MgO, testifying to their typical incompatible behaviour during komatiite lava differentiation. Data for Re from both flows define two almost indistinguishable trends that pass through the olivine compositions and, thus, represent olivine control lines. There are several TN samples that plot above the regression line, including TN7 and ZV14. Apparently, in these samples Re was mobilized during alteration. Both the Pt and Pd data for each lava flow define separate trends that pass either through, or close to the respective olivine compositions. As such, these regressions represent olivine control lines, providing evidence that both Pt and Pd were immobile during alteration, and that their variations in the lava flows were controlled solely by olivine.

The HSE abundances in the emplaced lavas at both localities, calculated from the ISOPLOT regressions for each element using the MgO content in the emplaced lavas (Fig. 5), are presented in Table 4. The emplaced lava of the TN flow contained (ppb): 0.52 Re, 1.5 Os, 1.3 Ir, 5.3 Ru, 9.3 Pt, and 8.7 Pd, as compared to 0.46 Re, 2.4 Os, 2.1 Ir, 5.2 Ru, 10.8 Pt, and 10.3 Pd in the PH flow. The emplaced la-

Table 3
HSE abundances (ppb) and elemental ratios in the TN and PH flows.

Sample	Re	Os	Ir	Ru	Pt	Pd	Re/Ir	Os/Ir	Ru/Ir	Pt/Ir	Pd/Ir
TN flow											
TN1	0.543	1.72	1.55	5.29	9.64	8.47	0.350	1.11	3.41	6.22	5.46
TN3	0.565	0.489	0.510	4.88	11.0	10.2	1.11	0.959	9.56	21.6	20.0
TN5	0.566	0.601	0.576	4.82	10.3	9.68	0.983	1.04	8.37	17.9	16.8
TN6	0.653	0.380	0.439	4.36	12.0	10.2	1.49	0.866	9.93	27.2	23.3
ZV14	0.767	0.351	0.451	3.96	13.0	11.4	1.70	0.779	8.78	28.8	25.4
TN7	0.903	2.02	1.66	5.94	7.62	7.88	0.545	1.22	3.59	4.60	4.76
TN10	0.432	2.10	1.76	5.82	8.09	7.72	0.245	1.19	3.30	4.59	4.38
TN12	0.372	2.21	1.80	5.95	6.85	6.92	0.207	1.23	3.31	3.81	3.85
TN14	0.379	2.66	2.17	6.08	6.86	6.66	0.175	1.23	2.80	3.16	3.07
TN15	0.368	2.34	1.94	5.73	6.94	6.64	0.190	1.21	2.96	3.58	3.43
TN16A	0.370	3.27	2.63	6.08	6.25	6.64	0.141	1.24	2.53	2.38	2.53
TN16B	0.344	3.75	3.09	5.94	6.24	6.34	0.111	1.21	1.92	2.02	2.05
TN17A	0.348	2.62	2.17	5.96	6.31	6.38	0.160	1.21	2.75	2.91	2.94
TN17B	0.342	2.98	2.45	6.01	6.14	6.31	0.140	1.22	2.45	2.51	2.58
TN18A	0.352	3.15	2.56	5.96	6.48	6.39	0.138	1.23	2.33	2.53	2.50
TN18B	0.353	3.43	2.84	6.05	6.46	6.43	0.124	1.21	2.13	2.27	2.26
TN18C	0.361	3.46	2.82	5.79	6.39	6.42	0.128	1.23	2.05	2.26	2.27
TN19A	0.394	2.60	2.17	5.80	7.43	6.84	0.181	1.20	2.67	3.42	3.15
TN19B	0.505	2.74	2.27	5.62	7.13	6.87	0.223	1.21	2.48	3.14	3.03
TN19C	0.527	3.09	2.53	5.69	7.12	6.81	0.208	1.22	2.25	2.81	2.69
TN20	0.374	2.41	2.00	5.75	6.57	6.68	0.187	1.21	2.88	3.29	3.35
TN21A	0.457	2.99	2.50	6.01	7.94	7.67	0.182	1.20	2.40	3.17	3.06
TN21B	0.440	2.85	2.43	5.70	7.81	7.04	0.181	1.17	2.35	3.22	2.90
TN21C	0.441	2.47	2.16	5.35	7.91	7.24	0.204	1.14	2.47	3.66	3.35
TN21D	0.432	2.65	2.33	5.88	8.17	7.44	0.186	1.14	2.53	3.51	3.20
ZV10A	0.482	2.39	1.96	5.72	9.04	8.16	0.246	1.22	2.92	4.62	4.17
ZV10B	0.471	2.15	1.79	5.38	9.09	7.78	0.264	1.21	3.01	5.09	4.36
ZV10 Chr	0.591	22.0	15.3	336	3.89	17.4	0.0387	1.44	22.0	0.254	1.13
ZV10 Ol	0.00349	3.61	2.63	6.51	0.193	0.132	0.00133	1.37	2.47	0.0733	0.0500
PH flow											
PH25A	0.465	2.60	2.17	5.09	10.9	9.70	0.214	1.20	2.35	5.02	4.47
PH25B	0.462	2.67	2.22	5.10	10.7	9.62	0.208	1.20	2.29	4.81	4.33
PH26	0.471	2.01	1.72	4.75	10.3	10.2	0.274	1.16	2.76	5.98	5.89
PH28	0.548	1.97	1.71	4.94	11.2	10.5	0.320	1.15	2.89	6.53	6.17
PH30A	0.304	6.93	5.38	5.29	8.19	7.33	0.0564	1.29	0.98	1.52	1.36
PH30B	0.304	6.26	4.82	5.27	8.06	7.31	0.0630	1.30	1.09	1.67	1.52
PH30C	0.309	6.43	4.95	5.24	8.04	7.32	0.0623	1.30	1.06	1.62	1.48
PH31A	0.252	6.75	5.21	5.16	7.64	6.81	0.0483	1.30	0.99	1.47	1.31
PH31B	0.252	7.40	5.54	5.08	7.83	6.94	0.0455	1.34	0.92	1.41	1.25
PH31C	0.254	6.93	5.21	5.03	7.91	7.06	0.0487	1.33	0.96	1.52	1.36

Note. The analyses are re-calculated on an anhydrous basis.

vas of the TN and PH flows, thus, have identical Os/Ir (1.14 ± 0.11 and 1.15 ± 0.11), and similar Re and Ru concentrations. The absolute Os and Ir concentrations, however, are ~60% higher, and Pt and Pd ~20% higher in the emplaced lava of the PH flow.

4.3. Re–Os isotopic data

The Re–Os isotopic data for the TN and PH flows obtained in this study are presented in Table 5. These new data, together with the Re–Os data for the PH flow from Puchtel et al. (2004a) are plotted on Re–Os isochron diagrams in Fig. 6. The Re–Os data for twenty four whole-rock samples, including 10 replicates, and olivine and chromite separates from the TN flow, define a regression line with a slope corresponding to an age of 2689 ± 16 Ma, and an initial $^{187}Os/^{188}Os = 0.10836 \pm 32$ ($\gamma^{187}Os = -0.22 \pm 0.30$). Three samples collected from just above and right below the B_1 subzone in the TN flow plot well below the regression line and, thus, contain some excess Re not supported by respective ingrowth of ^{187}Os. These samples also have Re concentrations that plot above the olivine control line in Fig. 5, indicating some later movement of Re, likely due to secondary alteration, and were not included into the regression calculations. Some Re mobility in several other samples is also inferred from the scatter of the data about the regression line that cannot be accounted for by the analytical uncertainty, as indicated by the MSWD = 13. This regression line does not meet the robust criteria for an isochron, since the MSWD value exceeds the maximum expected value of 1.6 calculated for the given degree of freedom (26) using the protocol of Wendt and Carl (1991).

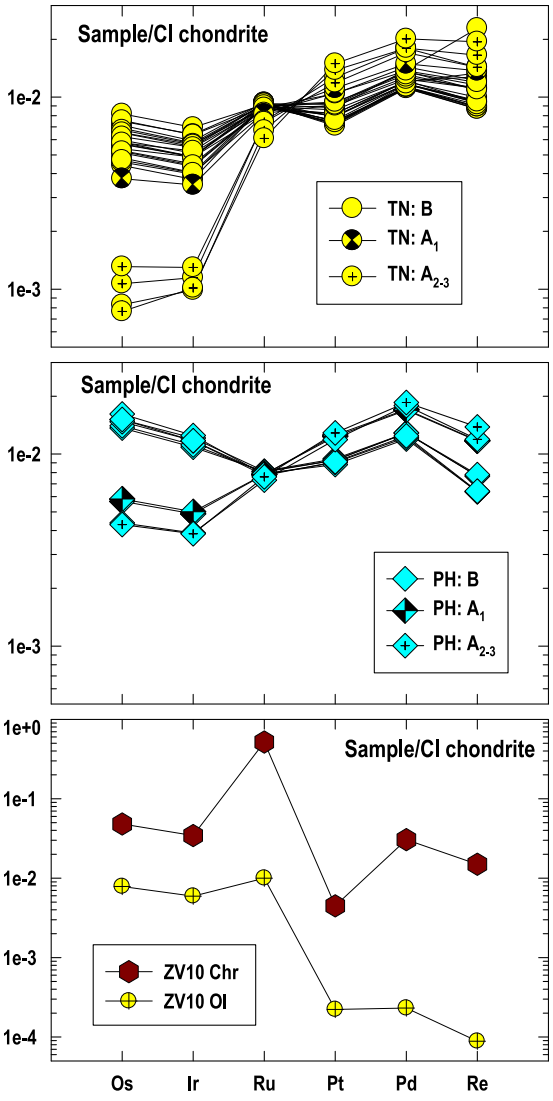

Fig. 4. CI chondrite-normalized (Horan et al., 2003) HSE abundances in whole-rock samples from the TN and PH flows and olivine and chromite separates from the TN flow.

The cumulate sample ZV10, its two replicates, and pure olivine and chromite fractions separated from this sample define a well-constrained (MSWD = 0.4) and precise internal isochron with an age of 2690 ± 16 Ma and an initial $^{187}Os/^{188}Os = 0.10875 \pm 17$, corresponding to an initial $\gamma^{187}Os = +0.14 \pm 0.16$. Both Re–Os ages are identical to the Pb–Pb isochron age of 2692 ± 9 Ma interpreted to represent the emplacement age of the Reliance Formation (Chauvel et al., 1993). This initial ratio represents our best estimate of the initial $^{187}Os/^{188}Os$ in the source of the TN flow. Using an early solar system initial $^{187}Os/^{188}Os = 0.09531$ (Shirey and Walker, 1998) and the ^{187}Re decay constant $\lambda = 1.666 \times 10^{-11}$ year^{-1} (Smoliar et al., 1996), it is calculated that the source of the TN flow would have evolved from $T = 4558$ Ma to its initial $^{187}Os/^{188}Os = 0.10875$ at 2690 Ma with a time-integrated, chondritic $^{187}Re/^{188}Os = 0.407 \pm 5$.

The initial $^{187}Os/^{188}Os = 0.10875 \pm 17$ obtained in this study is ~2.5% lower than the initial $^{187}Os/^{188}Os = 0.11140 \pm 84$ obtained by Walker and Nisbet (2002). In their study, these authors analyzed both whole-rock samples and olivine and chromite separates from the Onias's and Tony's flows. The whole-rock Re–Os data showed a highly disrupted, open-system behaviour, with initial $\gamma^{187}Os$ ranging between −2.1 and −410, which was interpreted to be the result of Re-remobilization due to intrusion of Proterozoic dolerites, likely associated with a major flood basalt event in Zimbabwe. As a result, only data for olivine and chromite separates were used for regression calculations by these authors. These data plot with a substantial scatter, unaccounted for by the analytical uncertainty (MSWD = 18), about the regression line with a slope corresponding to an age of 2721 ± 21, consistent with the accepted emplacement age of the lavas, but yielded an initial $\gamma^{187}Os = +2.8 \pm 0.8$. At present, the source of the discrepancy is not clear. In contrast to the results of Walker and Nisbet (2002), our whole-rock Re–Os data show much less scatter and essentially immobile behaviour of Re during secondary alteration. This could be due to the fact that in the present study, we homogenized substantially larger rock volumes during sample preparation stage, and also used better preserved drill core samples, which may have aided in negating the effects of small-scale Re-redistribution during the Proterozoic thermal event. Second, due to the substantial improvements in the analytical techniques over the past decade, the total analytical blanks in this study were about an order of magnitude lower than those in Walker and Nisbet (2002). Due to the very low Re concentrations in the chromite separates analyzed by Walker and Nisbet (2002), the calculated Re blank contributions were between 100% and 4000%. Such large uncertainties on the Re abundances may have resulted in over-correction of Re abundances and for the ^{187}Os ingrowth in the separates; the extremely low Re concentrations in the chromite separates analyzed by Walker and Nisbet (2002), compared to that from our study, support this conclusion.

The Re–Os data for 10 whole-rock samples, including five replicates, from the PH flow are approximated by a well-constrained (MSWD = 0.5) and precise isochron with an age of 2737±16 Ma and an initial $^{187}Os/^{188}Os = 0.10860 \pm 12$, corresponding to an initial $\gamma^{187}Os = +0.32 \pm 0.10$. This age and the initial ratio are identical to those we calculated using ISOPLOT 3.00 for the set of five samples from the Puchtel et al. (2004a) study (2719 ± 54 Ma, $\gamma^{187}Os = +0.61 \pm 0.28$). Regression of the data from the present study, together with those from Puchtel et al. (2004a), produces a statistically indistinguishable, albeit more precise, isochron (MSWD = 1.8) with an age of 2733 ± 20 Ma and an initial $^{187}Os/^{188}Os = 0.10873 \pm 15$, corresponding to a $\gamma^{187}Os(T) = +0.40 \pm 0.14$. This represents our best estimate of the initial $^{187}Os/^{188}Os$ in the source of the PH komatiites. The source of the PH flow is calculated to have evolved to its initial $^{187}Os/^{188}Os = 0.10873$ at 2733 Ma with a time-integrated, chondritic $^{187}Re/^{188}Os = 0.415 \pm 5$.

4.4. Pt–Os isotopic data

The new Pt–Os isotopic data for the TN and PH flows, together with those for the PH flow from the Puchtel et al.

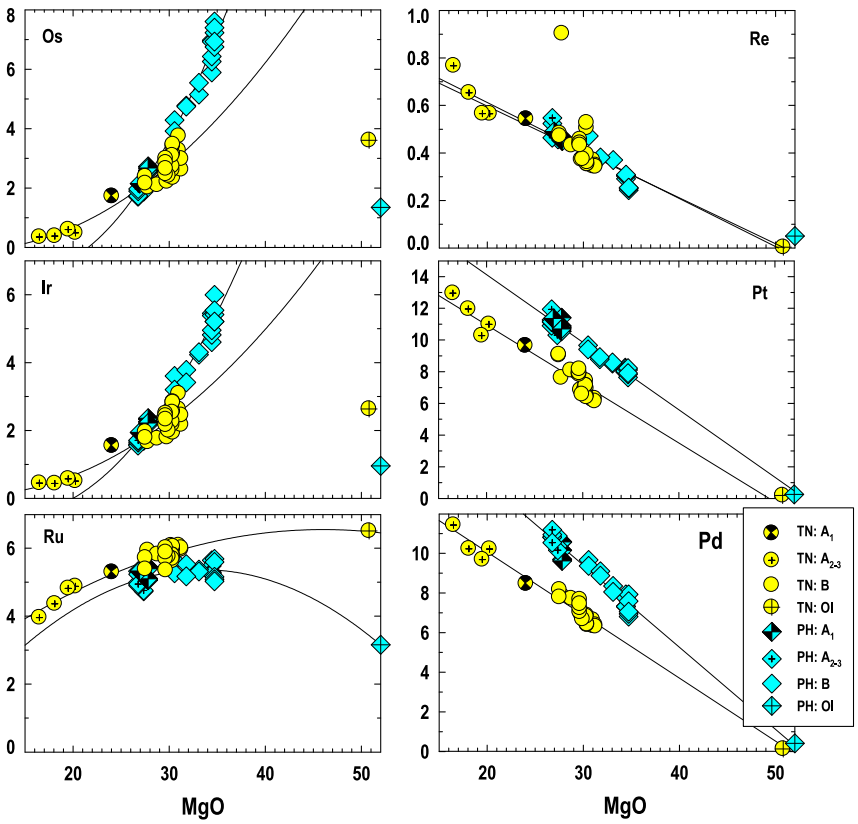

Fig. 5. Variations of HSE abundances as a function of MgO content in whole-rock komatiite samples and olivine separates from the TN and PH flows. Data for the PH flow also include those from Puchtel et al. (2004b).

Table 4
Calculated HSE abundances (ppb) and MgO (wt.%) in emplaced komatiite lavas and mantle sources of the TN and PH flows. The PUM estimate from Becker et al. (2006) is provided for comparison.

	Re	Os	Ir	Ru	Pt	Pd	MgO
Emplaced lavas							
TN	0.52 ± 0.08	1.5 ± 0.1	1.3 ± 0.1	5.3 ± 0.1	9.3 ± 0.8	8.7 ± 0.5	24.5 ± 0.5
PH	0.46 ± 0.07	2.4 ± 0.2	2.1 ± 0.2	5.2 ± 0.1	10.8 ± 0.5	10.3 ± 0.6	27.8 ± 0.5
Sources							
TN	0.24 ± 0.04	2.8 ± 0.4	2.5 ± 0.4	5.8 ± 0.5	4.1 ± 0.4	4.3 ± 0.3	38.0
PH	0.24 ± 0.04	2.8 ± 0.4	2.4 ± 0.4	5.7 ± 0.5	6.4 ± 0.3	6.1 ± 0.4	38.0
PUM	0.35 ± 0.12	3.9 ± 1.0	3.5 ± 0.8	7.0 ± 1.8	7.6 ± 2.6	7.1 ± 2.6	38.0

Note. The uncertainties are $2\sigma_{mean}$.

(2004a) study, are given in Table 6 and are plotted on Pt–Os isochron diagrams in Fig. 7. Four samples from the TN flow define an isochron with an age of 2805 ± 277 Ma and an initial $^{186}Os/^{188}Os = 0.1198315 \pm 7$, corresponding to an initial $\varepsilon^{186}Os = 0.00 \pm 0.06$. Since the initial $^{186}Os/^{188}Os$ ratio calculated from the isochron is strongly influenced by the uncertainty on the isotopic composition of the single sample (ZV10) that controls the slope of the isochron, a more accurate way of estimating the initial $^{186}Os/^{188}Os$ ratio of the source of the lavas is to average the initial $^{186}Os/^{188}Os$ ratios for each sample, calculated for the emplacement age of the lavas, and using the measured Pt/Os and $^{186}Os/^{188}Os$ ratios. The average initial $^{186}Os/^{188}Os$ ratio, calculated in this way, is 0.1198318 ± 3 (initial $\varepsilon^{186}Os = 0.01 \pm 0.03$) and represents our best estimate of the initial $^{186}Os/^{188}Os$ in the source of the TN komatiites. Using an early solar system initial $^{186}Os/^{188}Os = 0.1198269$ (Brandon et al., 2006) and the ^{190}Pt decay constant $\lambda = 1.477 \times 10^{-12}$ year^{-1} (Begemann et al., 2001), it is calculated that the source of the TN flow would evolve from $T = 4558$ Ma to its initial $^{186}Os/^{188}Os = 0.1198318$ at 2690 Ma with a time-integrated, chondritic $^{190}Pt/^{188}Os = 0.00178 \pm 0.00011$, equivalent to $Pt/Os = 1.86 \pm 0.12$.

The Pt–Os data for three samples from the PH flow analyzed in this study define an isochron with an age of

Table 5
Re–Os isotopic data for the TN and PH flows.

Sample	Re (ppb)	Os (ppb)	$^{187}Re/^{188}Os$	$^{187}Os/^{188}Os$	$\gamma^{187}Os(T)$
TN flow					
TN1	0.5091	1.617	1.527	0.17771 ± 16	−0.8
TN3	0.5443	0.4707	5.751	0.37241 ± 27	0.3
TN5	0.5478	0.5818	4.652	0.32159 ± 26	−0.1
TN6	0.6347	0.3693	8.664	0.48358 ± 37	−20
ZV14	0.7463	0.3413	11.16	0.57965 ± 56	−37
TN7	0.8780	1.961	2.164	0.15335 ± 09	−50
TN10	0.4163	2.024	0.9945	0.15355 ± 07	−0.6
TN12	0.3613	2.145	0.8136	0.14530 ± 06	−0.5
TN14	0.3688	2.589	0.6874	0.13799 ± 10	−1.9
TN15	0.3603	2.294	0.7584	0.14233 ± 26	−0.9
TN16A	0.3588	3.171	0.5456	0.13301 ± 09	−0.5
TN16B	0.3333	3.636	0.4419	0.12891 ± 09	0.1
TN17A	0.3347	2.521	0.6406	0.13782 ± 07	−0.1
TN17B	0.3292	2.868	0.5536	0.13403 ± 07	0.1
TN18A	0.3376	3.023	0.5385	0.13372 ± 15	0.4
TN18B	0.3382	3.284	0.4964	0.13125 ± 15	−0.1
TN18C	0.3460	3.321	0.5025	0.13171 ± 09	0.1
TN19A	0.3838	2.533	0.7317	0.14230 ± 12	0.2
TN19B	0.4918	2.664	0.7011	0.14072 ± 10	0.0
TN19C	0.5137	3.010	0.6179	0.13710 ± 09	0.2
TN20	0.3658	2.355	0.7498	0.14146 ± 14	−1.4
TN21A	0.4379	2.869	0.7367	0.14125 ± 12	−1.0
TN21B	0.4220	2.733	0.7455	0.14254 ± 16	−0.2
TN21C	0.4230	2.365	0.8643	0.14825 ± 15	0.0
TN21D	0.4147	2.542	0.7877	0.14485 ± 13	0.1
ZV10A	0.4721	2.337	0.9769	0.15338 ± 06	0.0
ZV10B	0.4615	2.107	1.059	0.15739 ± 10	0.2
ZV10 Chr	0.5915	22.03	0.1291	0.11462 ± 18	0.1
ZV10 Ol	0.003495	3.606	0.004659	0.10900 ± 10	0.2
PH flow					
PH-25A	0.4350	2.430	0.8649	0.14877 ± 09	0.1
PH-25B	0.4326	2.500	0.8358	0.14762 ± 09	0.3
PH-26	0.4405	1.876	1.137	0.16172 ± 12	0.4
PH-28	0.5154	1.852	1.349	0.17135 ± 10	0.2
PH-30A	0.2787	6.352	0.2112	0.11852 ± 10	0.4
PH-30B	0.2784	5.741	0.2335	0.11960 ± 11	0.4
PH-30C	0.2833	5.896	0.2313	0.11951 ± 11	0.4
PH-31A	0.2306	6.187	0.1792	0.11687 ± 13	0.2
PH-31B	0.2311	6.782	0.1639	0.11626 ± 10	0.3
PH-31C	0.2325	6.350	0.1761	0.11673 ± 10	0.2

Note. A–D are separate digestions of the same sample powders. The initial $\gamma^{187}Os$ were calculated for the ages of 2690 (TN) and 2733 Ma (PH). The Re and Os concentrations are not re-calculated on an anhydrous basis.

2630 ± 406 Ma and an initial $^{186}Os/^{188}Os = 0.1198315 \pm 13$. In this study, we replicated samples PH30 and PH31 analyzed by Puchtel et al. (2004a). Data for sample PH31 from Puchtel et al. (2004a) overlap within analytical uncertainty with those from this study, whereas the data for sample PH30 do not. The replicate of PH30 from this study plots on the regression line obtained by Puchtel et al. (2004a), whereas the previously analyzed sample PH30 plotted well above the regression line. Regression of all the Pt–Os data with the exception of the single outlier yields an isochron with an age of 2728 ± 443 Ma and an initial $^{186}Os/^{188}Os = 0.1198316 \pm 9$, corresponding to an initial $\varepsilon^{186}Os = 0.00 \pm 0.08$. The average of initial $^{186}Os/^{188}Os$ ratios of all samples is calculated to be 0.1198316 ± 5 (initial $\varepsilon^{186}Os = 0.00 \pm 0.04$). This initial ratio represents our best estimate of the initial $^{186}Os/^{188}Os$ in the source of the PH komatiites. The source of the PH flow would have evolved from the early solar system to its initial $^{186}Os/^{188}Os = 0.1198316$ at 2733 Ma with a time-integrated, chondritic $^{190}Pt/^{188}Os = 0.00174 \pm 0.00018$, which is equivalent to a $Pt/Os = 1.82 \pm 0.19$. The Pt–Re–Os data, thus, indicate that both the time-integrated Re/Os and Pt/Os in the sources of the TN and PH flows were identical within uncertainties.

4.5. Sm–Nd isotopic data

The Sm–Nd data for the TN flow are presented in Table 7. The Sm/Nd ratios in the six $A_{1\text{-}3}$ and $B_{2\text{-}4}$ samples analyzed are identical within 1.1%. Since both Sm and Nd

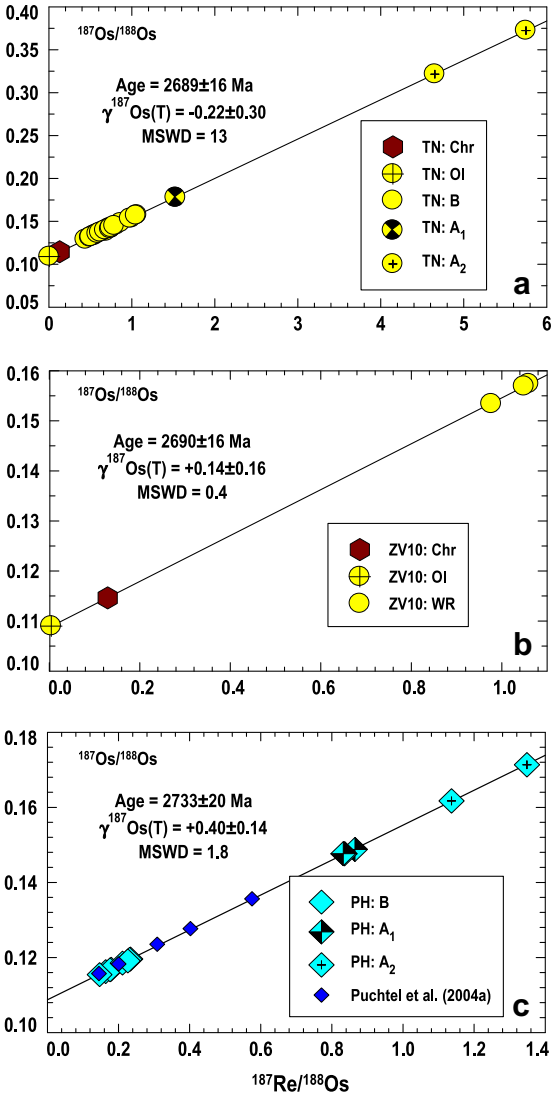

Fig. 6. Re–Os isotopic data for the TN whole-rock samples and olivine and chromite separates (a and b) and for the PH whole-rock samples (c). Data for the PH komatiites from this study obtained at the *IGL* and those obtained at the *JSC* (Puchtel et al., 2004a) are shown by separate symbols.

are characterized by similarly low partition coefficients between olivine and komatiite liquid (e.g., Arndt and Lesher, 1992), and as olivine was the only major fractionating mineral phase in the TN flow, these results are consistent with closed-system post-emplacement behaviour. The initial ε^{143}Nd values calculated for the emplacement age of 2692 Ma are nearly identical for all samples and average $+2.9 \pm 0.1$ ($2\sigma_{mean}$). This indicates that the source of the Belingwe komatiites evolved with a time-integrated suprachondritic Sm/Nd, e.g., it was depleted in highly incompatible lithophile trace elements, such as LREE, long before the formation of the Belingwe komatiite. Since the Pyke Hill komatiites have identical initial $\varepsilon^{143}\text{Nd} = +2.9 \pm 0.2$ (Puchtel et al., 2004a), the remarkable similarity between the sources of the two komatiite systems in terms of the Pt–Re–Os systematics, thus, also extends to the lithophile element isotope systematics.

5. DISCUSSION

5.1. Origin of the Belingwe and Abitibi komatiite sources

The TN and PH komatiites are characterized by $(Ce/Sm)_N = 0.68 \pm 0.01$and 0.52 ± 0.01, respectively, indicating that their mantle sources were strongly depleted in highly incompatible trace elements, and, thus, presumably also water. McDonough and Ireland (1993) concluded, on the basis of their study of trace element abundances in glass inclusions in olivines from Belingwe komatiites, that they are ancient analogues of modern, plume-derived, anhydrous magmas. Canil (1997) reported data for V partitioning between glass inclusions and host olivine in Belingwe komatiites that indicate that the oxidation state of these lavas, as well as several other komatiites, such as those from Abitibi and Kambalda, was very similar to that of present-day plume-derived oceanic island basalts. Using our V data for the TN flow, we calculate a bulk differentiation solid–liquid $D^V = 0.04 \pm 0.02$, which is identical to that of Canil (1997). Finally, studies of the oxidation state of iron in melt inclusions from the Belingwe komatiites indicated derivation from a dry source, similar to that of MORB (Berry et al., 2008). Based on these cumulative data, we conclude that both the TN and PH lavas formed via anhydrous melting. As such, using the compositions of the emplaced TN and PH komatiite lavas and the protocol of Nisbet et al. (1993a) and Abbott et al. (1994), we calculate the liquidus temperatures of these lavas to be 1525 ± 20 °C and 1565 ± 20 °C, respectively. This compares with the average liquidus temperatures of ~1520 °C calculated by Nisbet et al. (1993a) for the komatiites sampled in the SASKMAR drill core. These liquidus temperatures are translated into potential mantle temperatures of 1740 ± 20 °C and 1780 ± 20 °C, using the protocol of McKenzie and Bickle (1988) and Abbott et al. (1994), with the depths of melting initiation of ~250 and 375 km for the TN and PH komatiites, respectively. These sources were, thus, ~220 °C and 260 °C hotter than the temperature of the contemporary ambient mantle predicted by secular cooling models (*ca.* 1520 °C: Richter, 1988). Such conditions, whereby the ascending material is >200 °C hotter than the ambient mantle, are consistent with those projected for mantle plumes (e.g., Herzberg et al., 2007). Our data are, therefore, most consistent with a mantle plume origin for both the TN and PH komatiites.

5.2. HSE abundances in the Belingwe and Abitibi komatiite sources

Constraints on the absolute and relative HSE abundances in the mantle sources of the TN and PH flows can be obtained from the Pt–Re–Os isotope systematics and HSE abundances in the lavas. The Pt–Re–Os isotope systematics of the lavas afford time-integrated Pt/Os and Re/Os ratios in the sources, whereas the HSE abundances in the lavas provide clues regarding absolute HSE concentrations in the mantle sources at the time of formation of the lavas.

In order to calculate the absolute abundances of the HSE in the komatiite sources, we used a projection tech-

Table 6
Precise osmium isotopic data and Re/Os and Pt/Os ratios for the TN and PH flows.

Sample	$^{187}Re/^{188}Os$	$^{190}Pt/^{188}Os$	$^{184}Os/^{188}Os$	$^{186}Os/^{188}Os$	$^{187}Os/^{188}Os$	$\gamma^{187}Os(T)$	$\varepsilon^{186}Os(T)$
TN flow							
TN16[b]	**0.5834**	**0.002010**	**0.0013125 ± 10**	**0.1198399 ± 13**	**0.1351753 ± 13**	**−0.15 ± 0.13**	**0.02 ± 0.11**
TN18[a]	**0.5856**	**0.001909**	**0.0013153 ± 35**	**0.1198389 ± 21**	**0.1355657 ± 32**	**0.12 ± 0.12**	**−0.04 ± 0.18**
TN19[a]	**0.6775**	**0.002639**	**0.0013078 ± 32**	**0.1198423 ± 33**	**0.1396180 ± 31**	**-0.04 ± 0.14**	**0.01 ± 0.28**
ZV10[b]	**1.0491**	**0.003898**	**0.0013131 ± 09**	**0.1198476 ± 13**	**0.1568930 ± 14**	**0.17 ± 0.23**	**0.03 ± 0.11**
PH flow							
PH25[a]	**0.8322**	**0.003959**	**0.0013135 ± 34**	**0.1198468 ± 20**	**0.1476556 ± 18**	**0.52 ± 0.18**	**-0.06 ± 0.17**
PH29		0.002407	0.0013097 ± 18	0.1198422 ± 11	0.1347934 ± 21		0.07 ± 0.09
PH30		0.001309	0.0013102 ± 21	0.1198392 ± 12	0.1192968 ± 10		0.19 ± 0.10
PH30[b]	**0.2264**	**0.001196**	**0.0013070 ± 10**	**0.1198365 ± 15**	**0.1190932 ± 14**	**0.25 ± 0.05**	**0.01 ± 0.12**
PH31		0.001128	0.0013086 ± 13	0.1198359 ± 11	0.1152762 ± 08		−0.02 ± 0.09
PH31[b]	**0.1469**	**0.001057**	**0.0013070 ± 07**	**0.1198355 ± 10**	**0.1154453 ± 10**	**0.30 ± 0.03**	**−0.04 ± 0.08**
PH32		0.001511	0.0013087 ± 24	0.1198375 ± 13	0.122539 ± 27		−0.02 ± 0.11
PH33		0.001993	0.0013091 ± 26	0.1198406 ± 06	0.127730 ± 13		0.08 ± 0.05

Note. The uncertainties on the Re/Os and Pt/Os ratios are 0.5% relative. Boldfaced values – present study; the high-precision measurements were performed at either the *IGL* (a), or at the *JSC* (b). The rest of the data are from (Puchtel et al., 2004a). The initial $\varepsilon^{186}Os$ were calculated for the ages of 2690 (TN) and 2733 Ma (PH).

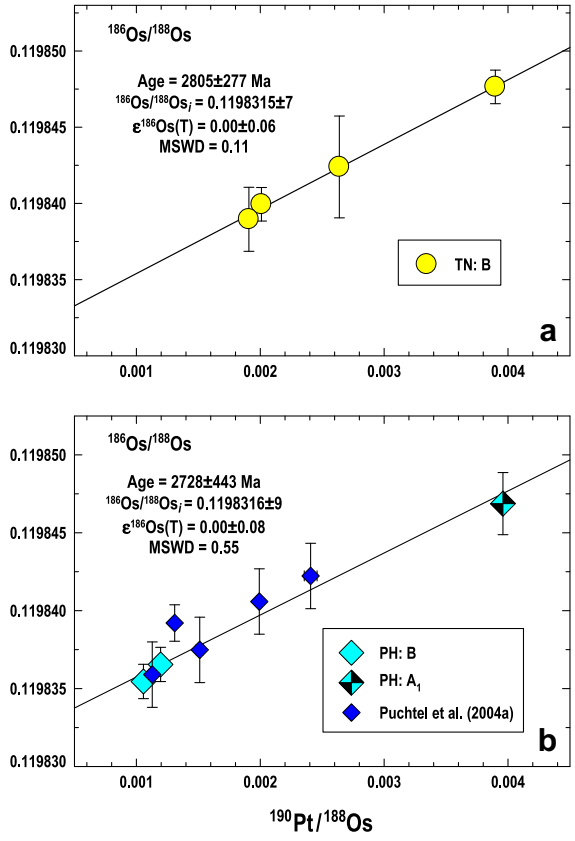

Fig. 7. Pt–Os isotopic data for the TN (a) and PH (b) flows. The data for the PH flow from Puchtel et al. (2004a) are shown by separate symbols.

nique that has been previously applied to the Abitibi, Kostomuksha, and Volotsk komatiites (Puchtel et al., 2004a, 2004b; Puchtel and Humayun, 2005; Puchtel et al., 2007), with some modifications. The technique is based on the assumption that a mineral phase behaves similarly during low-pressure partial melting in the mantle source and crystallization of the lava after emplacement, i.e., the last residual mineral phase that enters the melt would be the first to crystallize. Thus, if an HSE was incompatible with the low-pressure residual mineral assemblage during melting that produced the lava, it was also likely similarly incompatible with the liquidus mineral assemblage during differentiation of an emplaced komatiite lava. For a specific komatiite lava suite, the abundances of elements that are incompatible with the residue (i.e., the mineral hosts of these elements have been exhausted during melting) should plot on the liquidus lines of descent drawn through the data for the lavas, and source HSE concentrations can be calculated for a given MgO content in the source. Since the MgO content of the mantle is little affected by previous melt extractions, Puchtel et al. (2004b) used MgO = 38% in an average depleted spinel peridotite (ADSL), which is also the accepted MgO content in the putative Primitive Mantle of McDonough and Sun (1995). It should be noted, however, that the S content at saturation of a mafic lava increases with decreasing pressure, so magmas become undersaturated during adiabatic ascent (Mavrogenes and O'Neill, 1999). As a result, the bulk HSE partition coefficients of the first phases to fractionate could differ from those that last enter the melt during partial melting. This limitation can only be lifted if there is no sulfide left in the source after melting. Therefore, one of the pre-requisites for our protocol to be applicable for calculating the HSE composition of the mantle source of a lava from its HSE abundances is the complete exhaustion of sulfide in the source during partial melting. This can only be attained if the degree of melting exceeds ~25% (Barnes et al., 1985; Hamlyn et al., 1985; Keays, 1995). Therefore, this protocol cannot be applied to relatively low-degree melts, such as MORB, which form via <30% melting. The only exceptions are melts formed under relatively high oxygen fugacity. For example, Mungall et al. (2006) reported high, unfractionated HSE concentrations in small-degree partial melts such as meimechites.

Table 7
Sm–Nd isotopic data for the TN flow.

Sample	Sm, ppm	Nd, ppm	$^{147}Sm/^{144}Nd$	$^{143}Nd/^{144}Nd$	$\varepsilon^{143}Nd(T)$
TN1	0.6386	1.735	0.2226	0.513240 ± 7	+2.8
TN3	0.7659	2.092	0.2214	0.513228 ± 6	+3.0
TN4	0.7419	2.010	0.2231	0.513253 ± 6	+2.9
TN6	0.8603	2.327	0.2235	0.513260 ± 6	+2.9
TN19	0.4945	1.340	0.2230	0.513252 ± 6	+2.9
ZV10	0.5911	1.596	0.2239	0.513268 ± 6	+2.9

Note. Initial $\varepsilon^{143}Nd$ were calculated for the emplacement age $T = 2690$ Ma. The Sm and Nd concentrations are not re-calculated on an anhydrous basis.

They showed that these melts can be produced via relatively low-degree melting that takes place at moderately high oxygen fugacity, which will reduce the amount of sulfide due to the formation of sulfate and will also destabilize residual monosulfide solid solution by driving sulfide melts into the spinel-liquid di-variant field. These authors argued that magmas formed at high oxygen fugacity by small degrees of mantle melting can be important agents for the transfer of chalcophile elements from the upper mantle to the crust and may be progenitors of significant ore deposits of Pt, Pd, and Au. The degrees of partial melting estimated for the TN and PH komatiites on the basis of the incompatible trace element data are 35% and 50%, respectively. Under these conditions, sulfide in the sources would likely have been completely exhausted. Thus, to estimate the abundances of the incompatible HSE (Re, Pt, and Pd) in the sources of these komatiites, we extrapolate the trends of each of these elements to an MgO content of 38 wt.%. Using this protocol, the concentrations of incompatible Re in both TN and PH sources were calculated to be 0.24 ± 0.04 ppb. The Pt abundances were calculated to be 4.1 ± 0.4 and 6.4 ± 0.3 ppb, and Pd abundances to be 4.3 ± 0.2 and 6.1 ± 0.4 ppb in the sources of the TN and PH flows, respectively (Table 4).

The concentrations of compatible Os were obtained using the calculated Re contents in the sources and the time-integrated $^{187}Re/^{188}Os$ derived from the initial $^{187}Os/^{188}Os$. The calculated Os concentrations are 2.8 ± 0.4 for both the TN and PH sources. The Ir abundances in the sources were calculated from the Os contents and the Os/Ir in the emplaced lavas, which have been shown to have retained the Os/Ir ratios of the sources during high degrees of partial melting (Puchtel and Humayun, 2000; Puchtel et al., 2004b). The Ir contents are calculated to be 2.5 ± 0.4 and 2.4 ± 0.4 for the TN and PH sources, respectively. Finally, to calculate the Ru abundances in the sources, we used the compositions of emplaced komatiite lavas and the observation that the bulk solid–liquid partition coefficient during komatiite melting and differentiation is close to unity ($D^{Ru} = 1.1 \pm 0.1$: Puchtel et al., 2004b). The Ru abundances are, thus, calculated to be 5.8 ± 0.5 and 5.7 ± 0.5 ppb in the TN and PH sources, respectively. It should be noted that, because the Os abundances were calculated from the time-integrated Re/Os of the sources of the lavas, these calculated Os (and Ir) abundances in the sources represent time-integrated Os abundances, not abundances at the time of melting. However, because of the very compatible nature of Os (and Ir) during low-degrees of partial melting, such as that involved in generation of basalts, the melting residue left after basalt extraction that ultimately gave rise to the komatiite magmas would have had virtually unchanged Os (and Ir) abundances and would, thus, approximate the Os (and Ir) abundances at the time of melting.

The CI chondrite-normalized HSE concentrations in the TN and PH komatiite sources are plotted in Fig. 8, together with those for the Primitive Upper Mantle (PUM) estimate of Becker et al. (2006). Although we acknowledge the purely hypothetical nature of the PUM reservoir, which likely does not exist in real world, we find it useful to compare the HSE abundances in the komatiite sources with a theoretical HSE composition for this putative reservoir, because it presents a certain standard against which the variability created in natural mantle sources by billions of years of geological processes can be tested. The IPGE and Re abundances estimated for the komatiite sources overlap with the PUM estimate, although they are at the lower end of the range for PUM. The PPGE abundances in the PH source overlap with those in the PUM estimate, whereas Pd, and especially Pt, abundances in the TN source are resolvably lower than those in the PUM.

5.3. The lithophile *vs*. highly siderophile element systematics

There is a potential conflict between the strong depletions in highly incompatible lithophile trace elements, such as, e.g., LREE, and the generally chondritic Re/Os in the sources of komatiites throughout most of geologic history. For instance, the sources of the 3.3 Ga Commondale (Wilson et al., 2003), 2.9 Ga Volotsk (Puchtel et al., 2007), 2.0 Ga Lapland (Gangopadhyay et al., 2006), 250 Ma Vietnam (Hanski et al., 2004), and 89 Ma Gorgona komatiites (Walker et al., 1999) have basically the same features: near-chondritic time-integrated Re/Os and strong long-term depletions in LREE. Thus, solving this problem using high-precision HSE komatiite data will have relevance to the evolution of the entire mantle throughout geologic history.

The time-integrated subchondritic Nd/Sm in the sources of both the TN and PH komatiites indicate that these sources underwent episodes of melting and melt extraction a minimum of several hundred Ma prior to formation of the komatiite sequences. As a result, the mantle domains that gave rise to the TN and PH komatiites were depleted in Nd vs. Sm and, by the same token, should have been depleted in other incompatible elements relative to less incom-

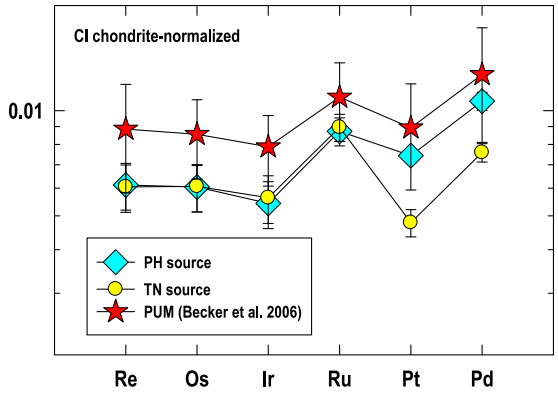

Fig. 8. CI chondrite-normalized (Horan et al., 2003) HSE abundances in the calculated mantle sources of the TN and PH komatiites and in the PUM estimate of Becker et al. (2006). The uncertainties are 2σ.

patible. Re is generally incompatible with terrestrial mantle residues and Os is normally strongly compatible, so it might be expected that the melt extraction events that generated the subchondritic Nd/Sm, would also have produced subchondritic Re/Os in the residue, which would then have resulted in retardation of the ingrowth of ^{187}Os in the latter, compared to ambient mantle. Yet, the time-integrated Re/Os in the sources of the TN and PH komatiites remain well within the range of chondritic meteorites. An attempt to reconcile this apparent paradox for the Pyke Hill and Volostsk komatiite sources was made by Puchtel et al. (2004b) and Puchtel et al. (2007) via utilizing a model whereby the sources experienced low degrees of partial melting and melt extraction several hundred Ma prior to the emplacement of the lavas. Their modelling showed that Re/Os was not sufficiently modified by low extents of melting such that its effect would be isotopically resolvable from chondritic evolution. Their modelling was based on the assumption that Re partitioning during mantle melting was similar to that of Yb, based on the results of experimental work performed at a very low oxygen fugacity (Righter and Hauri, 1998). These redox conditions, however, have been recently argued to be inappropriate for generation of most terrestrial magmas (Mallmann and O'Neill, 2007). Mallmann and O'Neill (2007) have shown that the crystal-silicate melt partition coefficients for Re decrease by several orders of magnitude, as its oxidation state changes from +4 (common for MORB) to +6 (typical of island arc basalts, IAB). They argued that even at its lowest oxidation state, Re^{4+} partitioning behaviour is more similar to that of Ti^{4+} than Yb. Therefore, Re may be more strongly incompatible than previously believed. If so, this may invalidate the modelling of Puchtel et al. (2004a).

To further investigate the apparent discrepancy between lithophile trace element and the HSE behaviour in komatiite sources over the Earth's history, the evolution of the Sm–Nd and Re–Os isotope systematics of the TN and PH komatiite sources are modelled here using the new Re partitioning data. The assumptions and parameters used in the modelling are as follow: (1) the mantle reservoir that was subjected to the initial melting and melt extraction had a composition consistent with that of model PUM. The REE and HSE parameters of this model PUM reservoir were compiled from the data of O'Nions et al. (1977), Jacobsen and Wasserburg (1980), Hamilton et al. (1983), Hofmann (1988), Meisel et al. (2001), and Becker et al. (2006). (2) The model PUM reservoir had a composition of spinel lherzolite (65% Ol, 24% Opx, 10% Cpx, 1% Sp, 0.3% Sulf) and the melting was described by the batch melting equation of Shaw (1970). (3) The bulk D^{Sm} and D^{Nd} during melting are calculated to be 0.037 and 0.023, respectively, using the above modal mineral composition and crystal–liquid D from Green (1994). (4) The bulk D^{Re} during batch melting of this model reservoir under redox conditions appropriate for the formation of dry komatiite magmas is conservatively estimated to be 0.2 (Fonseca et al., 2007; Mallmann and O'Neill, 2007), as compared with the value of 0.3 used in the prior model of Puchtel et al. (2004a). Using this bulk D^{Re}, a Re content in a typical MORB lava formed by 8% batch melting of this model PUM reservoir is calculated to be ca. 1.3 ppb, which is consistent with the average Re content of MORB glasses (e.g., Escrig et al., 2005). The bulk Os partition coefficient for low-degree melting was defined to be 50 (e.g., Roy-Barman et al., 1998; Escrig et al., 2005).

We model evolution of the Sm–Nd and Re–Os isotopic systematics for two mantle melting scenarios. The first scenario considers the latest possible (youngest), single-stage, maximum-degree of melting events that would appropriately fractionate the Sm/Nd in the PUM reservoir from the chondritic value to those calculated for the komatiite sources and bring the ε^{143}Nd values of these reservoirs to +2.9 by the time of komatiite formation at 2.7 Ga. The collateral effects on the Re–Os isotope system resulting from the Nd isotope-based constraints are then considered using parameters gleaned from the Sm–Nd modelling. In the second scenario, we consider the effects of an early, global differentiation event that is consistent with recent hypotheses based on the short-lived ^{146}Sm–^{142}Nd isotope system (e.g., Boyet and Carlson, 2006). This scenario requires the minimum-degree of melting (or other process) that would lead to fractionation of Sm/Nd in the PUM reservoir from the chondritic value to that required to bring the ε^{143}Nd of the reservoir to +2.9 by the time the komatiites formed (2.7 Ga).

For scenario (1), we first calculate the maximum ^{147}Sm/^{144}Nd ratios in the TN and PH komatiite sources to be 0.2306 and 0.2674, respectively, based on the REE data for the respective lavas, and using the projection technique of calculating incompatible element abundances in komatiite sources outlined above. On the basis of these ratios, modelling establishes that prior melting events could have generated the initial ε^{143}Nd values of +2.9 at 2.7 Ga via removal of ~1.4% melt from a PUM reservoir at ~3.4 Ga for the TN source, and via removal of ~5% melt at ~3.2 Ga for the PH source. Using these extents and times of melting, and applying the bulk $D^{Re} = 0.2$, we calculate that the melting events that produced these LREE depletions would have reduced the ^{187}Re/^{188}Os by 7% in the PUM for the TN source (i.e., from 0.424 to 0.396), and by 26% in the PUM for the PH source (i.e., from 0.424 to

0.336). The projected minor reduction in Re/Os in the PUM for the TN source would allow generation of the observed $^{187}Os/^{188}Os$ from a source with a long-term Re/Os that is slightly higher (0.436) than the PUM estimate (0.424), albeit just within the range of chondritic meteorites (see Fig. 9). However, the projected major reduction in Re/Os in the PUM for the PH source would not allow the generation of the observed chondritic $^{187}Os/^{188}Os$ from any source which had long-term Re/Os within the range of chondritic meteorites.

Is it possible that a komatiite source prior to initial melting could have had a long-term suprachondritic Re/Os? The observation that the abundances of the HSE in the mantle are considerably higher than would result from low-pressure metal-silicate partitioning has led to speculation that mantle HSE abundances were established at high pressures and temperatures at which the HSE may not be so highly siderophile, such as at the base of a magma ocean (e.g., Murthy, 1991; Righter et al., 2000), or as a result of continued (late) accretion of materials with average chondritic compositions following cessation of core segregation (Kimura et al., 1974; Chou et al., 1983; Morgan et al., 2001). The most recent high-temperature metal-silicate Os partitioning data of Brenan and McDonough (in press) require very low Os abundances in the silicate portion of the Earth following core formation. These data, when considered together with the high-temperature partitioning data for Re (Ohtani and Yurimoto, 1996) and Pt (Cottrell and Walker, 2006) require very suprachondritic Re/Os (~8000) and Pt/Os (~40,000) in the silicate Earth following core segregation. The high absolute and generally chondritic relative abundances of the HSE in the mantle, therefore, indicate that the HSE signature imparted to the silicate Earth as a result of last equilibration between metallic core and silicate portion of the Earth has been lost.

On the other hand, Os isotopic data for some lunar impact melt rocks, formed as a result of basin-forming events, indicate that at least some sizable impactors had Re/Os as much as 20% greater than the currently known range of chondritic meteorites (Fig. 9). It is also known that the impactors that created the largest impact basins on the surface of the Moon, and presumably the Earth, too, were tens of km in diameter (Ryder, 2002; Strom et al., 2005) and, thus, once assimilated by the mantle, would be capable of generating large HSE heterogeneities. These heterogeneities could have persisted for several hundred million years in the mantle following the impacts and could have been tapped by plumes that gave rise to komatiites. The major shortcoming of this scenario is that it requires a set of very specific circumstances, whereby mantle sources with variably enriched Re/Os each evolved in a specific way to match the chondritic reference at exactly the time when each komatiite was formed. Although not impossible, this scenario is considered highly unlikely.

For scenario (2), we assume that a melting event occurred within 100 Ma of the Earth's accretion. Using an extrapolated chondritic $^{143}Nd/^{144}Nd = 0.506829$ at 4.50 Ga, it is calculated that the sources of the TN and PH flows would evolve from this value to their initial $^{143}Nd/^{144}Nd$ at 2.7 Ga with time-integrated $^{147}Sm/^{144}Nd = 0.2092 \pm 2$ and 0.2095 ± 2, respectively. This modest change in $^{147}Sm/^{144}Nd$ from the chondritic ratio of 0.1967 by partial melting would require only ~0.4% melting and removal of the resulting melt. At the same time, this degree of melting and melt extraction would have decreased the $^{187}Re/^{188}Os$ in the residue by only ~2% (from 0.424 of PUM to 0.416). The resulting $^{187}Re/^{188}Os$ would be, thus, well within the range permitted by the chondritic requirements for the sources of the TN and PH komatiites calculated from their Re–Os isotope systematics.

Consideration of this type of early-Earth differentiation event affecting the Sm–Nd isotope system has recently gained attention as a result of $^{142,143}Nd/^{144}Nd$ studies of a wide range of terrestrial rocks and chondritic meteorites (Boyet et al., 2003; Boyet and Carlson, 2006; Caro et al., 2006; Bennett et al., 2007). For example, Boyet and Carlson (2006) suggested that both oceanic and continental crust might have been derived from a mantle reservoir that had been depleted in highly incompatible elements very early in Earth history. The highly incompatible elements would have been incorporated into a hidden reservoir (proto crust?) shortly after the Earth's formation. The resulting depleted reservoir would have persisted likely throughout Earth's history, and would currently occupy between 75 and >90% of the mantle (Carlson and Boyet, 2008). Boyet and Carlson (2006) noted that both the ^{142}Nd and ^{143}Nd isotopic systematics of the depleted mantle (with a present-day $\varepsilon^{143}Nd$ value of +8.5 to 11) can be accounted for by an early differentiation event if it left a depleted mantle with a $^{147}Sm/^{144}Nd$ ratio of 0.209–0.216 within 5–60 Ma of the start of the solar system. The projected $^{147}Sm/^{144}Nd$ in both TN and PH komatiitic sources are within this range.

Although the $^{142,143}Nd$ data are consistent with a global differentiation event that took place within several tens of million years after accretion, the mechanism of differentiation remains very poorly constrained. The initial differentiation event could have occurred as a result of partial melting and melt removal from a large portion of the mantle over a relatively short period of time, or formation and subsequent solidification of a terrestrial magma ocean. The Re–Os isotopic results are consistent with this interpretation if the depleted reservoir formed via shallow melting followed by melt removal. The effects of magma ocean differentiation on the Re/Os systematics, however, are currently difficult to project. As discussed below, however, this may not matter.

This scenario (2), single-stage early melting model, however, does not resolve all issues with our data. First, in order for the komatiite sources to acquire the elevated $^{147}Sm/^{144}Nd$ ratios of 0.2306 (TN) or 0.2674 (PH) calculated from the REE data for the lavas, a second depletion event would be required. This can be envisaged as a depletion event that occurred very shortly before or during the melting that ultimately produced the TN and PH komatiites, so that it would not have had any effect on their Nd and Os isotopic systematics. Since in Archean greenstone belt sequences komatiites are usually associated with tholeiites, this second-stage melting might have involved first formation and removal of tholeiitic basalts, followed by melting of the further depleted source to produce the

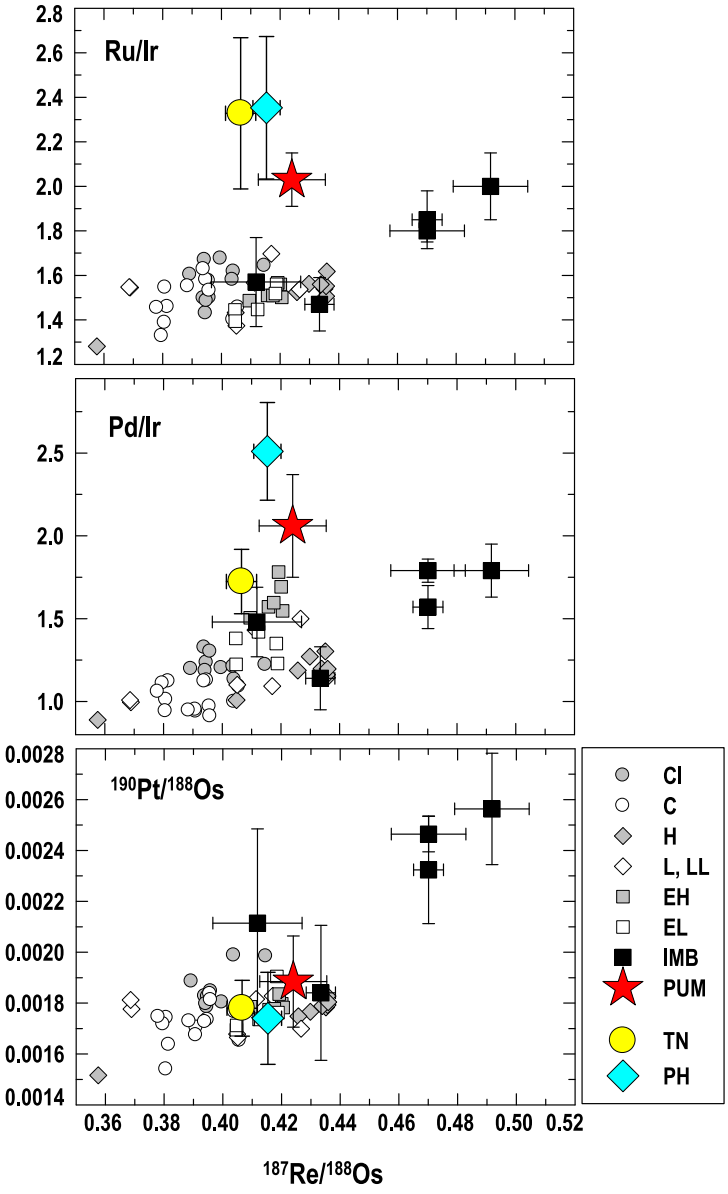

Fig. 9. Variations of Re/Os vs. Ru/Ir, Pd/Ir, and Pt/Os in the calculated sources of the TN and PH komatiites as compared to those in chondritic meteorites (Walker et al., 2002; Horan et al., 2003; Brandon et al., 2005a, 2005b), PUM estimates (Meisel et al., 2001; Becker et al., 2006), and lunar impact melt breccias, IMB (Puchtel et al., 2008). The uncertainties are 2σ.

komatiites, similar to the dynamic melting in a mantle plume head model proposed by Campbell et al. (1989) and Arndt et al. (1997). Hence, this observation is not difficult to account for.

A second problem relates to the timing of the putative depletion event in relation to subsequent events that could have overprinted residual HSE abundances. Although the results of Boyet and Carlson (2006) allow the ^{142,143}Nd data to be explained by extraction events occurring within 60 Ma of Solar System formation, the best solution is within 10 Ma, potentially long before the addition of the HSE to the upper mantle via continued accretion of planetesimals (late veneer). It has been generally accepted that the Moon formed via the giant impact of a Mars-sized body onto the proto-Earth (Canup and Asphaug, 2001). The similarity of ^{182}W isotope compositions between the Earth and Moon (Touboul et al., 2009) suggests that this event occurred at least 50 Ma following Solar System formation, thus, potentially postdating the hypothesized initial differentiation event. The lunar-forming impact would have led to considerable (complete?) melting of the mantle, a rain of metal through the molten mantle, and fresh extraction of HSE into the newly merged cores of the Earth and impactor. Thus, the establishment of HSE abundances in the terrestrial mantle by late accretion likely did not occur until long after the initial differentiation event (e.g. Walker, 2009). Hence, the HSE in the komatiite sources may not have been established by the initial differentiation event projected by

the Nd isotopic data, but by later mantle fractionation or late accretionary processes. This interpretation, however, is permissible, as long as the secondary giant impact event did not lead to mixing of the incompatible element-enriched reservoir back into the depleted mantle.

5.4. The significance of the suprachondritic CaO/Al_2O_3 in the TN and PH komatiites

Both the TN and PH komatiites belong to the so-called Al-undepleted type of lavas that are characterized by chondritic Al_2O_3/TiO_2, Ti/Y, Zr/Y, or Gd/Yb, indicative of a complete lack of garnet in their mantle source residues. However, the CaO/Al_2O_3 in these lavas are ~30% higher than that in the PM. This suprachondritic Ca/Al has been argued by some authors to reflect the transient feature of the primitive convecting mantle derived by 10–15% crystal fractionation of an assemblage comprised by Mg-perovskite, Ca-perovskite, and ferropericlase in the proportions 93:3:4 from a magma ocean with bulk silicate Earth composition (Walter et al., 2004). This primitive convecting mantle would also have been expected to acquire suprachondritic Sm/Nd and Lu/Hf during the differentiation event, and with time develop radiogenic Nd and Hf isotopic compositions, as discussed by Caro et al. (2005) and Shirey et al. (2008). This scenario is consistent with the observed very early LREE-depletions in the TN and PH komatiites. From the Re–Os standpoint, however, this scenario is presently difficult to evaluate due to the lack of Re partitioning data for the mineral phases that are stable at the bottom of a magma ocean conditions.

6. CONCLUDING REMARKS

The unique properties of komatiites make HSE from komatiitic lavas potentially much more representative of their mantle sources than the HSE from basalts or mantle xenoliths. Archean komatiites in particular provide information about the HSE abundances in the mantle at a time when the mantle was undoubtedly less modified by processes of melt extraction and refertilization via crustal recycling, compared to the modern mantle. The precise Pt–Re–Os isotopic and HSE abundance data, together with the Sm–Nd isotopic and REE data obtained in this study for well preserved 2.7 Ga komatiite lavas from the Belingwe (TN) and Abitibi (PH) greenstone belts, characterize their respective mantle sources. These parameters by far represent the most precise estimates of time-integrated Sm/Nd, Pt/Os, and Re/Os of the Archean mantle and provide evidence for the remarkable similarity of the two sources with respect to both REE and HSE. The emplaced komatiite lavas contained ~25% (TN) and ~28% (PH) MgO and were likely derived via dry melting of mantle plume sources that were >200 °C hotter than the ambient mantle, and were characterized by strong, long-term depletions in LREE. Yet, the calculated HSE abundances in their mantle sources were generally within the range of the PUM estimates, and the precise time-integrated Re/Os and Pt/Os in their sources are best matched by those in enstatite chondrites. The apparent discrepancy between the highly siderophile and lithophile trace element and isotope systematics of the two komatiite sources are best reconciled via a two-stage melting model. The initial moderate depletions in LREE were created as a result of very early magma ocean differentiation or extraction and isolation of early crust, consistent with the recent ^{142}Nd–^{143}Nd isotopic data obtained for a wide range of terrestrial rocks and chondritic meteorites. These events either had a negligible effect on the HSE budget of the mantle, or their effects were overprinted by subsequent late accretion of materials with chondritic bulk HSE abundances. The second, larger-degree melting events that produced the more pronounced LREE depletions in the sources tapped by the TN and PH komatiites, must have occurred nearly contemporaneously with the formation of the komatiites, likely as a result of dynamic melting in mantle plumes. These results might have relevance to the evolution of the entire mantle throughout geologic history.

ACKNOWLEDGMENTS

We thank Tony Martin, who discovered the freshest Reliance Fm. outcrop, for generous long-term collaboration and ongoing support. We are thankful to Mike Lesher and Rebecca Sproule for help with collecting drill core samples from the Pyke Hill area and to Martin Menzies for editorial handling. The final version of the manuscript has greatly benefitted from thoughtful and constructive reviews by Steve Shirey and Nick Arndt. This work was made possible through the support by the NSF Grant EAR-0635690 to ISP; this support is gratefully acknowledged.

REFERENCES

Abbott D. H., Burgess L., Longhi J. and Smith W. H. F. (1994) An empirical thermal history of the Earth's upper mantle. *J. Geophys. Res.* **99**, 13835–13850.

Arndt N. T., Naldrett A. J. and Pyke D. R. (1977) Komatiitic and iron-rich tholeiitic lavas of Munro Township, northeast Ontario. *J. Petrol.* **18**, 319–369.

Arndt N. T. (1986) Differentiation of komatiite flows. *J. Petrol.* **27**, 279–301.

Arndt N. T. and Lesher C. M. (1992) Fractionation of REE's by olivine and the origin of Kambalda komatiites, Western Australia. *Geochim. Cosmochim. Acta* **56**, 4191–4204.

Arndt N. T., Kerr A. C. and Tarney J. (1997) Dynamic melting in plume heads: the formation of Gorgona komatiites and basalts. *Earth Planet. Sci. Lett.* **146**, 289–301.

Arndt N. T., Lesher C. M. and Barnes S. J. (2008) *Komatiite*. Cambridge University Press, Cambridge, UK.

Ayer J. A., Amelin Y., Corfu F., Kamo S., Ketchum J., Kwok K. and Trowell N. (2002) Evolution of the southern Abitibi greenstone belt based on U–Pb geochronology: autochthonous volcanic construction followed by plutonism, regional deformation and sedimentation. *Precambrian Res.* **115**, 63–95.

Barnes S.-J., Naldrett A. J. and Gorton M. P. (1985) The origin of the fractionation of platinum-group elements in terrestrial magmas. *Chem. Geol.* **53**, 303–323.

Beattie P., Ford C. and Russell D. (1991) Partition coefficients for olivine-melt and orthopyroxene-melt systems. *Contrib. Mineral. Petrol.* **109**, 212–224.

Becker H., Horan M. F., Walker R. J., Gao S., Lorand J.-P. and Rudnick R. L. (2006) Highly siderophile element composition of the Earth's primitive upper mantle: constraints from new

data on peridotite massifs and xenoliths. *Geochim. Cosmochim. Acta* **70**, 4528–4550.

Begemann F., Ludwig K. R., Lugmair G. W., Min K., Nyquist L. E., Patchett P. J., Renne P. R., Shih C.-Y., Villa I. M. and Walker R. J. (2001) Call for an improved set of decay constants for geochronological use. *Geochim. Cosmochim. Acta* **65**, 111–121.

Bennett V. C., Brandon A. D. and Nutman A. P. (2007) Coupled ^{142}Nd–^{143}Nd isotopic evidence for Hadean mantle dynamics. *Science* **318**, 1907–1910.

Berry A. J., Danyushevsky L. V., O'Neill H. S. C., Newville M. and Sutton S. R. (2008) Oxidation state of iron in komatiitic melt inclusions indicates hot Archaean mantle. *Nature* **455**, U942–U960.

Bickle M. J., Martin A. and Nisbet E. G. (1975) Basaltic and peridotitic komatiites and stromatolites above a basal unconformity in the Belingwe greenstone belt, Rodesia. *Earth Planet. Sci. Lett.* **27**, 155–162.

Bickle M. J., Arndt N. T., Nisbet E. G., Orpen J. L., Martin A., Keays R. R. and Renner R. (1993) Geochemistry of the igneous rocks of the Belingwe Greenstone Belt: alteration, contamination and petrogenesis. In The Geology of the Belingwe Greenstone Belt, Zimbabwe. A study of the Evolution of Archaean Continental Crust (eds. M. J. Bickle, E. G. Nisbet). *Geol. Soc. Zimbabwe Spec. Publ.*, pp. 175–213.

Birck J. L., Roy-Barman M. and Capman F. (1997) Re–Os isotopic measurements at the femtomole level in natural samples. *Geostand. Newslett.* **20**, 19–27.

Boyet M., Blichert-Toft J., Rosing M., Storey M., Télouk P. and Albarède F. (2003) ^{142}Nd evidence for early Earth differentiation. *Earth Planet. Sci. Lett.* **214**, 427–442.

Boyet M. and Carlson R. W. (2006) A new geochemical model for the Earth's mantle inferred from ^{146}Sm–^{142}Nd systematics. *Earth Planet. Sci. Lett.* **250**, 254–268.

Brandon A. D., Snow J. E., Walker R. J., Morgan J. W. and Mock T. D. (2000) ^{190}Pt–^{186}Os and ^{187}Re–^{187}Os systematics of abyssal peridotites. *Earth Planet. Sci. Lett.* **177**, 319–335.

Brandon A. D., Humayun M., Puchtel I. S., Leya I. and Zolensky M. (2005a) Osmium isotope evidence for an s-process carrier in primitive chondrites. *Science* **309**, 1233–1236.

Brandon A. D., Humayun M., Puchtel I. S. and Zolensky M. (2005b) Re–Os isotopic systematics and platinum group element composition of the Tagish Lake carbonaceous chondrite. *Geochim. Cosmochim. Acta* **69**, 1619–1631.

Brandon A. D., Walker R. J. and Puchtel I. S. (2006) Platinum-osmium isotope evolution of the Earth's mantle: constraints from chondrites and Os-rich alloys. *Geochim. Cosmochim. Acta* **70**, 2093–2103.

Brenan J. M. and McDonough W. F. (in press) Core formation and metal-silicate fractionation of osmium and iridium from gold. *Nature.*

Campbell I. H., Griffiths R. W. and Hill R. I. (1989) Melting in an Archaean mantle plume: head it's basalts, tails it's komatiites. *Nature* **339**, 697–699.

Canil D. (1997) Vanadium partitioning and the oxidation state of Archaean komatiite magmas. *Nature* **389**, 842–845.

Canup R. M. and Asphaug E. (2001) Origin of the Moon in a giant impact near the end of the Earth's formation. *Nature* **412**, 708–712.

Carlson R. W. and Boyet M. (2008) Composition of the Earth's interior: the importance of early events. *Philos. Trans. Roy. Soc. Math. Phys. Eng. Sci.* **366**, 4077–4103.

Caro G., Bourdon B., Wood B. J. and Corgne A. (2005) Trace-element fractionation in Hadean mantle generated by melt segregation from a magma ocean. *Nature* **436**, 246–249.

Caro G., Bourdon B., Birck J.-L. and Moorbath S. (2006) High-precision ^{142}Nd/^{144}Nd measurements in terrestrial rocks: constraints on the early differentiation of the Earth's mantle. *Geochim. Cosmochim. Acta* **70**, 164–191.

Chauvel C., Dupré B. and Arndt N. T. (1993) Pb and Nd isotopic correlation in Belingwe komatiites and basalts. In *The Geology of the Belingwe Greenstone Belt, Zimbabwe. A Study of the Evolution of Archaean Continental Crust* (eds. M. J. Bickle, E. G. Nisbet). A.A. Balkema, Rotterdam/Brookfield, pp. 167–174.

Chou C.-L., Shaw D. M. and Crocket J. H. (1983) Siderophile trace elements in the Earth's oceanic crust and upper mantle. *J. Geophys. Res.* **88**(S2), A507–A518.

Cohen A. S. and Waters F. G. (1996) Separation of osmium from geological materials by solvent extraction for analysis by thermal ionisation mass spectrometry. *Anal. Chim. Acta* **332**, 269–275.

Cottrell E. and Walker D. (2006) Constraints on core formation from Pt partitioning in mafic silicate liquids at high temperatures. *Geochim. Cosmochim. Acta* **70**, 1565–1580.

Creaser R. A., Papanastassiou D. A. and Wasserburg G. J. (1991) Negative thermal ion mass-spectrometry of osmium, rhenium, and iridium. *Geochim. Cosmochim. Acta* **55**, 397–401.

Dupré B., Chauvel C. and Arndt N. T. (1984) Pb and Nd isotopic study of two Archean komatiitic flows from Alexo, Ontario. *Geochim. Cosmochim. Acta* **48**, 1965–1972.

Escrig S., Schiano P., Schilling J.-G. and Allegre C. (2005) Rhenium-osmium isotope systematics in MORB from the Southern Mid-Atlantic Ridge (40–50 S). *Earth Planet. Sci. Lett.* **235**, 528–548.

Fonseca R. O. C., Mallmann G., O'Neill H. S. C. and Campbell I. H. (2007) How chalcophile is rhenium? An experimental study of the solubility of Re in sulphide mattes. *Earth Planet. Sci. Lett.* **260**, 537–548.

Gangopadhyay A. and Walker R. J. (2003) Re–Os systematics of the ca. 2.7 Ga komatiites from Alexo, Ontario, Canada. *Chem. Geol.* **196**, 147–162.

Gangopadhyay A., Sproule R. A., Walker R. J. and Lesher C. M. (2005) Re–Os systematics of komatiites and komatiitic basalts at Dundonald Beach, Ontario, Canada: evidence for a complex alteration history and implications of a late-Archean chondritic mantle source. *Geochim. Cosmochim. Acta* **69**, 5087–5098.

Gangopadhyay A., Walker R. J., Hanski E. and Solheid P. (2006) Origin of paleoproterozoic komatiites at Jeesiörova, Kittilä greenstone complex, Finnish Lapland. *J. Petrol.* **47**, 773–789.

Green T. H. (1994) Experimental studies of trace-element partitioning applicable to igneous petrogenesis – Sedona 16 years later. *Chem. Geol.* **117**, 1–36.

Hamilton P. J., O'Nions R. K., Bridgwater D. and Nutman A. P. (1983) Sm–Nd studies of Archaean metasediments and metavolcanics from West Greenland and their implications for the Earth's early history. *Earth Planet. Sci. Lett.* **62**, 263–272.

Hamlyn P. R., Keays R. R., Cameron W. E., Crawford A. J. and Waldron H. M. (1985) Precious metals in magnesian low-Ti lavas: Implications for metallogenesis and sulfur saturation in primary magmas. *Geochim. Cosmochim. Acta* **49**, 1797–1811.

Handler M. R. and Bennett V. C. (1999) Behaviour of platinum-group elements in the subcontinental mantle of eastern Australia during variable metasomatism and melt depletion. *Geochim. Cosmochim. Acta* **63**, 3597–3618.

Hanski E., Walker R. J., Huhma H., Polyakov G. V., Balykin P. A., Hoa T. T. and Phuong N. T. (2004) Origin of the Permian-Triassic komatiites, northwestern Vietnam. *Contrib. Mineral. Petrol.* **147**, 453–469.

Herzberg C., Asimow P. D., Arndt N., Niu Y. L., Lesher C. M., Fitton J. G., Cheadle M. J. and Saunders A. D. (2007) Temperatures in ambient mantle and plumes: constraints from

basalts, picrites, and komatiites. *Geochem. Geophys. Geosyst.* **8,** Article Q02006.

Hofmann A. W. (1988) Chemical differentiation of the Earth: the relationship between mantle, continental crust and oceanic crust. *Earth Planet. Sci. Lett.* **90**, 297–314.

Horan M. F., Walker R. J., Morgan J. W., Grossman J. N. and Rubin A. E. (2003) Highly siderophile elements in chondrites. *Chem. Geol.* **196**, 5–20.

Huppert H. E. and Sparks R. S. J. (1985) Cooling and contamination of mafic and ultramafic magmas during ascent through continental crust. *Earth Planet. Sci. Lett.* **74**, 371–386.

Jacobsen S. B. and Wasserburg G. J. (1980) Sm–Nd isotopic evolution of chondrites. *Earth Planet. Sci. Lett.* **50**, 139–155.

Jones J. H. and Drake M. J. (1986) Geochemical constraints on core formation in the Earth. *Nature* **322**, 221–228.

Keays R. R. (1995) The role of komatiitic and picritic magmatism and S-saturation in the formation of ore deposits. *Lithos* **34**, 1–18.

Kimura K., Lewis R. S. and Anders S. (1974) Distribution of gold and rhenium between nickel-iron and silicate melts; implications for abundance of siderophile elements on the earth and moon. *Geochim. Cosmochim. Acta* **38**, 683–701.

Lahaye Y. and Arndt N. T. (1996) Alteration of a komatiite flow from Alexo, Ontario. *J. Petrol.* **37**, 1261–1284.

Lorand J. P., Alard O. and Godard M. (2009) Platinum-group element signature of the primitive mantle rejuvenated by melt–rock reactions: evidence from Sumail peridotites (Oman Ophiolite). *Terra Nova* **21**, 35–40.

Ludwig K. R. (2003) ISOPLOT 3.00. A geochronological toolkit for Microsoft Excel. *Berkeley Geochronology Center Spec. Publ.* No. 4: 70 pp.

Mallmann G. and O'Neill H. S. C. (2007) The effect of oxygen fugacity on the partitioning of Re between crystals and silicate melt during mantle melting. *Geochim. Cosmochim. Acta* **71**, 2837–2857.

Mavrogenes J. A. and O'Neill H. S. C. (1999) The relative effects of pressure, temperature and oxygen fugacity on the solubility of sulfide in mafic magmas. *Geochim. Cosmochim. Acta* **63**, 1173–1180.

McDonough W. F. and Ireland T. R. (1993) Intraplate origin of komatiites inferred from trace elements in glass inclusions. *Nature* **365**, 432–434.

McDonough W. F. and Sun S.-S. (1995) The composition of the Earth. *Chem. Geol.* **120**, 223–253.

McKenzie D. and Bickle M. J. (1988) The volume and composition of melt generated by extension of the lithosphere. *J. Petrol.* **29**, 625–679.

Meisel T., Walker R. J., Irving A. J. and Lorand J.-P. (2001) Osmium isotopic compositions of mantle xenoliths: a global perspective. *Geochim. Cosmochim. Acta* **65**, 1311–1323.

Mertzman S. A. (2000) K-Ar results from the southern Oregon – northern California Cascade range. *Oregon Geol.* **62**, 99–122.

Morgan J. W., Wanderless G. A., Petrie R. K. and Irving A. J. (1981) Composition of the earth's upper mantle, I. Siderophile trace elements in ultramafic nodules. *Tectonophysics* **75**, 47–67.

Morgan J. W. (1986) Ultramafic xenoliths: clues to Earth's late accretionary history. *J. Geophys. Res.* **91**, 12375–12387.

Morgan J. W., Walker R. J., Brandon A. D. and Horan M. F. (2001) Siderophile elements in Earth's upper mantle and lunar breccias: data synthesis suggests manifestations of the same late influx. *Meteor. Planet. Sci.* **36**, 1257–1275.

Mungall J. E., Hanley J. J., Arndt N. T. and Debecdelievre A. (2006) Evidence from meimechites and other low-degree mantle melts for redox controls on mantle-crust fractionation of platinum-group elements. *Proc. Natl. Acad. Sci. USA* **103**, 12695–12700.

Murthy V. R. (1991) Early differentiation of the Earth and the problem of mantle siderophile elements – a new approach. *Science* **253**, 303–306.

Nesbitt R. W. and Sun S.-S. (1976) Geochemistry of Archean spinifex-textured peridotites and magnesian and low-magnesian tholeiites. *Earth Planet. Sci. Lett.* **31**, 433–453.

Nisbet E. G., Bickle M. J. and Martin A. (1977) The mafic and ultramafic lavas of the Belingwe greenstone belt, Rodesia. *J. Petrol.* **18**, 521–566.

Nisbet E. G., Arndt N. T., Bickle M. J., Cameron W. E., Chauvel C., Cheadle M., Hegner E., Kyser T. K., Martin A., Renner R. and Roedder E. (1987) Uniquely fresh 2.7 Ga komatiites from the Belingwe greenstone belt, Zimbabwe. *Geology* **15**, 1147–1150.

Nisbet E. G., Cheadle M. J., Arndt N. T. and Bickle M. J. (1993a) Constraining the potential temperature of the Archaean mantle: A review of the evidence from komatiites. *Lithos* **30**, 291–307.

Nisbet E. G., Martin A., Bickle M. J. and Orpen J. L. (1993b) The Ngezi Group: komatiites, basalts and stromatolites on continental crust. In *The Geology of the Belingwe Greenstone Belt, Zimbabwe. A study of the Evolution of Archaean Continental Crust* (eds. M. J. Bickle and E. G. Nisbet). A.A. Balkema, Rotterdam/Brookfield, pp. 121–174.

O'Nions R. K., Hamilton P. J. and Evensen N. M. (1977) Variations in ^{143}Nd–^{144}Nd and ^{87}Sr–^{86}Sr Ratios in Oceanic Basalts. *Earth Planet. Sci. Lett.* **34**, 13–22.

Ohtani E. and Yurimoto H. (1996) Element partitioning between metallic liquid, magnesiowüstite, and silicate liquid at 20 GPa and 2500 °C – a secondary ion mass spectrometric study. *Geophys. Res. Lett.* **23**, 1993–1996.

Pearson D. G., Irvine G. J., Ionov D. A., Boyd F. R. and Dreibus G. E. (2004) Re–Os isotope systematics and platinum-group-element fractionation during mantle melt extraction: a study of massif and xenolith peridotite suites. *Chem. Geol.* **208**, 29–59.

Puchtel I. and Humayun M. (2000) Platinum group elements in Kostomuksha komatiites and basalts: implications for oceanic crust recycling and core–mantle interaction. *Geochim. Cosmochim. Acta* **64**, 4227–4242.

Puchtel I. S., Brandon A. D. and Humayun M. (2004a) Precise Pt–Re–Os isotope systematics of the mantle from 2.7-Ga komatiites. *Earth Planet. Sci. Lett.* **224**, 157–174.

Puchtel I. S., Humayun M., Campbell A., Sproule R. and Lesher C. M. (2004b) Platinum group element geochemistry of komatiites from the Alexo and Pyke Hill areas, Ontario, Canada. *Geochim. Cosmochim. Acta* **68**, 1361–1383.

Puchtel I. S., Brandon A. D., Humayun M. and Walker R. J. (2005) Evidence for the early differentiation of the core from Pt–Re–Os isotope systematics of 2.8-Ga komatiites. *Earth Planet. Sci. Lett.* **237**, 118–134.

Puchtel I. S. and Humayun M. (2005) Highly siderophile element geochemistry of ^{187}Os-enriched 2.8-Ga Kostomuksha komatiites, Baltic Shield. *Geochim. Cosmochim. Acta* **69**, 1607–1618.

Puchtel I. S., Humayun M. and Walker R. J. (2007) Os–Pb–Nd isotope and highly siderophile and lithophile trace element systematics of komatiitic rocks from the Volotsk suite, SE Baltic Shield. *Precambrian Res.* **158**, 119–137.

Puchtel I. S., Walker R. J., James O. B. and Kring D. A. (2008) Osmium isotope and highly siderophile element systematics of lunar impact melt breccias: Implications for the late accretion history of the Moon and Earth. *Geochim. Cosmochim. Acta* **72**, 3022–3042.

Pyke D. R., Naldrett A. J. and Eckstrand O. R. (1973) Archean ultramafic flows in Munro Township, Ontario. *Geol. Soc. Am. Bull.* **84**, 955–978.

Rehkämper M., Halliday A. N., Barfod D. and Fitton J. G. (1997) Platinum-group element abundance patterns in different mantle environments. *Science* **278**, 1595–1598.

Rehkämper M., Halliday A. N., Fitton J. G., Lee D.-C., Wieneke M. and Arndt N. T. (1999) Ir, Ru, Pt and Pd in basalts and komatiites: new constraints for the geochemical behavior of the platinum group elements in the mantle. *Geochim. Cosmochim. Acta* **63**, 3915–3934.

Renner R., Nisbet E. G., Cheadle M. J., Arndt N. T., Bickle M. J. and Cameron W. E. (1994) Komatiite flows from the reliance formation, Belingwe Belt, Zimbabwe: I. Petrography and mineralogy. *J. Petrol.* **35**, 361–400.

Richter F. M. (1988) A major change in the thermal state of the Earth at the Archean-Proterozoic boundary: consequences for the nature and preservation of continental lithosphere. *J. Petrol. Spec. Lithos. Issue* **3**, 9–52.

Righter K. and Hauri E. H. (1998) Compatibility of rhenium in garnet during mantle melting and magma genesis. *Science* **280**, 1737–1741.

Righter K., Walker R. J. and Warren P. H. (2000) Significance of highly siderophile elements and osmium isotopes in the lunar and terrestrial mantles. In *Origin of the Earth and Moon* (eds. K. Righter and R. M. Canup). University of Arizona Press, Tucson, pp. 291–322.

Roeder P. L. and Emslie R. F. (1970) Olivine-liquid equilibrium. *Contrib. Mineral. Petrol.* **29**, 275–282.

Roy-Barman M., Wasserburg G. J., Papanastassiou D. A. and Chaussidon M. (1998) Osmium isotopic compositions and Re–Os concentrations in sulfide globules from basaltic glasses. *Earth Planet. Sci. Lett.* **154**, 331–347.

Ryder G. (2002) Mass flux in the ancient Earth–Moon system and benign implications for the origin of life on Earth. *J. Geophys. Res.* **107,** 6.1–6.13.

Shaw D. M. (1970) Trace element fractionation during anatexis. *Geochim. Cosmochim. Acta* **40**, 73.

Shirey S. B. and Walker R. J. (1998) The Re–Os isotope system in cosmochemistry and high-temperature geochemistry. *Ann. Rev. Earth Planet. Sci.* **26**, 423–500.

Shirey S. B., Kamber B. S., Whitehouse M. J., Mueller P. A. and Basu A. R. (2008) A review of the isotopic and trace element evidence for mantle and crustal processes in the Hadean and Archean: implications for the onset of plate tectonic subduction. *Geol. Soc. Am. Spec. Paper* **440**, 1–29.

Smoliar M. I., Walker R. J. and Morgan J. W. (1996) Re–Os ages of Group IIA, IIIA, IVA, and IVB iron meteorites. *Science* **271**, 1099–1102.

Snow J. E. and Reisberg L. (1995) Os isotopic systematics of the MORB mantle: results from altered abyssal peridotites. *Earth Planet. Sci. Lett.* **136**, 723–733.

Sproule R. A., Lesher C. M., Ayer J. A., Thurston P. C. and Herzberg C. T. (2002) Spatial and temporal variations in the geochemistry of komatiites and komatiitic basalts in the Abitibi greenstone belt. *Precambrian Res.* **115**, 153–186.

Sproule R. A., Lesher C. M., Houle M. G., Keays R. R., Ayer J. A. and Thurston P. C. (2005) Chalcophile element geochemistry and metallogenesis of Komatiitic rocks in the Abitibi greenstone belt, Canada. *Econ. Geol.* **100**, 1169–1190.

Strom R. G., Malhotra R., Ito T., Yoshida F. and Kring D. A. (2005) The origin of planetary impactors in the inner Solar system. *Science* **309**, 1847–1850.

Touboul M., Kleine T., Bourdon B., Palme H. and Wieler R. (2009) Tungsten isotopes in ferroan anorthosites: implications for the age of the Moon and lifetime of its magma ocean. *Icarus* **199**, 245–249.

Walker R. J., Shirey S. B. and Stecher O. (1988) Comparative Re–Os, Sm–Nd and Rb–Sr isotope and trace element systematics for Archean komatiite flows from Munro Township, Abitibi belt, Ontario. *Earth Planet. Sci. Lett.* **87**, 1–12.

Walker R. J., Morgan J. W., Beary E. S., Smoliar M. I., Czamanske G. K. and Horan M. F. (1997) Applications of the ^{190}Pt–^{186}Os isotope system to geochemistry and cosmochemistry. *Geochim. Cosmochim. Acta* **61**, 4799–4807.

Walker R. J., Storey M., Kerr A. C., Tarney J. and Arndt N. T. (1999) Implications of ^{187}Os isotopic heterogeneities in a mantle plume: evidence from Gorgona Island and Curaçao. *Geochim. Cosmochim. Acta* **63**, 713–728.

Walker R. J., Horan M. F., Morgan J. W., Becker H., Grossman J. N. and Rubin A. E. (2002) Comparative ^{187}Re–^{187}Os systematics of chondrites: implications regarding early solar system processes. *Geochim. Cosmochim. Acta* **66**, 4187–4201.

Walker R. J. and Nisbet E. (2002) ^{187}Os isotopic constraints on Archean mantle dynamics. *Geochim. Cosmochim. Acta* **66**, 3317–3325.

Walker R. J. (2009) Highly siderophile elements in the Earth, Moon and Mars: update and implications for planetary accretion and differentiation. *Chemie der Erde* **69**, 101–125.

Walter M. J., Nakamura E., Tronnes R. G. and Frost D. J. (2004) Experimental constraints on crystallization differentiation in a deep magma ocean. *Geochim. Cosmochim. Acta* **68**, 4267–4284.

Wendt I. and Carl C. (1991) The statistical distribution of the mean squared weighted deviation. *Chem. Geol.* **86**, 275–285.

Wilson A. H., Shirey S. B. and Carlson R. W. (2003) Archaean ultra-depleted komatiites formed by hydrous melting of cratonic mantle. *Nature* **423**, 858–860.

Zhou M. F. (1994) PGE distribution in 2.7-Ga layered komatiite flows from the Belingwe greenstone belt, Zimbabwe. *Chem. Geol.* **118**, 155–172.

Associate editor: Martin A. Menzies